Use of Beta-Gamma Coincidence Detection to Improve the Quality of Transmission Scans for PET

Marie-Laure A. Camborde

Medical Physics Unit
McGill University, Montreal

September 2001

A thesis submitted to the Faculty of Graduate Studies and Research in partial fulfilment of the requirements of the degree of Master of Science

---

0-612-78840-7

ABSTRACT

The availability of accurately aligned, whole body, functional PET images has a significant impact on the diagnosis of malignant disease and on identifying and localizing metastasis. Gamma ray attenuation correction is essential in all quantitative PET studies.

The object of this study was to explore the possibility of using beta-gamma coincidence as an attenuation correction technique in order to improve transmission scan image quality.

This study consisted of testing and implementing a beta-gamma attenuation correction technique on an animal PET scanner. In its final form the system uses ^{68}Ge sources enclosed in plastic scintillator cylinders coupled to PMTs. The detection of positrons is activated by the energy loss in the scintillator medium. This system is used in coincidence with one of the animal PET scanner's BGO crystal detectors in order to acquire transmission scans.

RESUME

La disponibilité d'images précises en scannographie TEP fonctionnelle a un impact significatif sur le diagnostique des tumeurs malignes ainsi que sur l'identification et la localisation des métastases. La correction de l'atténuation des rayons gamma est essentielle dans toutes études TEP quantitatives. Aujourd'hui cette acquisition se fait le plus communément en deux dimensions avec des sources allongées en rotation.

L'objet de cette étude est la possibilité d'utiliser une coïncidence beta-gamma comme technique de correction d'atténuation dans le but d'améliorer la qualité des images de scannographie de transmission.

Cette étude consiste à tester et l'implémenter la technique beta-gamma sur une scannographie animale. Le système mis en place contient des sources de ^{68}Ge renfermer dans des cylindres de matières plastiques scintillantes couplés à des tubes photomultiplicateurs. La détection des positons est déclencher par leur énergie perdue dans la matière scintillante. Enfin le système est en coïncidence avec un détecteur de rayons gamma classique.

ACKNOWLEDGMENTS

I would like to thank my supervisor, Dr. Chris Thompson, for his constant support and advise throughout this project. This work would not have been possible without his guidance and expertise. I would particularly like to thank him for supporting my participation in the Canadian Organization of Medical Physicists Annual Meeting in Kelowna this year.

Thank-you to all the members of our lab, Nan Zhang, Francois Cayouette, Dylan Togane for their support and their contribution to a great working atmosphere. Et bien sur Khanh Nguyen grâce à qui le travail dans le laboratoire le soir et le week-end a toujours été agréable. I hope to remain good friends with all of them.

I would also like to thank the staff of the MNI radiochemistry department for all their assistance in supplying ^{11}C for my experiments. I would like to thank in particular, Dean Jolly, Shadreck Mzengeza and Myriam Kovacevic for their technical support as well as their humor, advise and friendship.

From the McGill University workshop I would like to thank Steve Kecani and Eddie del Campo for teaching me all the mechanical skills needed in the design and construction of the beta-gamma system.

Je voudrais également remercier ma famille pour leur constant soutient moral et affectif tout au long de ces deux années loin d'eux et dans toutes les decisions que j'ai prises jusqu'à aujourd'hui.

Finally I would like to thank Peter Petric without whom I would never have finished this work.

TABLE OF CONTENT

CHAPTER 1

PRINCIPLES OF POSITRON EMISSION TOMOGRAPHY

CHAPTER 3

OVERVIEW OF BETA-GAMMA COINCIDENCE SYSTEM

CHAPTER 4

TESTS PERFORMED ON THE BETA-GAMMA SYSTEM

CHAPTER 5

RESULTS AND DISCUSSION

List of Figures

List of Tables

List of Schematics

CHAPTER 1

PRINCIPLES OF POSITRON EMISSION TOMOGRAPHY

Positron Emission Tomography (PET) is a non-invasive functional imaging modality that provides clinical information about biomedical and physiologic processes in the body. This is accomplished by introducing biologically relevant compounds labelled with positron emitting radionuclides into the subject and imaging and quantifying their distribution as they travel through the physiological systems of interest. Unlike the anatomical images obtained with devices such as Computed Tomography (CT), the functional images obtained in PET are calibrated to be displayed in units of activity concentration per unit volume. PET is being increasingly used with F-18-fluorodeoxyglucose (FDG) to evaluate recurrent tumors and to stage cancer by assessing the existence of remote tumors as in the case of metastases.

I. INTRODUCTION

1. Radionuclides

Approximately 30 years ago, it was proven possible to localize a positron-emitting radionuclide by detecting the resulting annihilation photons [1]. The positrons emitted from these radionuclides annihilate with electrons after losing energy in the medium in which the positron is travelling. Two 511 keV photons are given off from each of these annihilations. In PET imaging, these annihilation photons are detected thus localizing the positron emitting source in order to form a functional image.

Figure 1 Annihilation process [2]

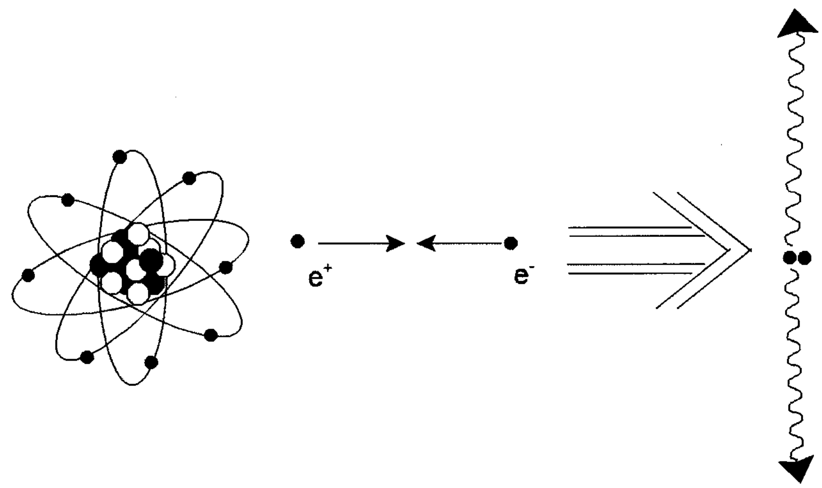

A wide range of positron emitting radionuclides with short half-lives are used in PET. In order to introduce these radionuclides into the appropriate physiological system, they must first be attached to an appropriate tracer compound. Substrates, ligands, drugs, antibodies, and neurotransmitters are frequently used for this purpose and are labelled with positron emitting radionuclides. These tracer compounds are then injected into or inhaled by the patient in order to reach the circulating blood. The main positron emitting radionuclides used in PET and their principle tracer compounds are listed in Table 1.

These elements are found in most of the compounds that are consumed by the human body which is one of the reasons why PET is so useful as a functional imaging technique. The high natural occurrence of these nuclides in the body enables for a large number of available tracer compounds which can be labelled and thus detected and followed through the body by PET. The short half-lives of these tracers are also very convenient in that they allow large doses to be administered to the patient with low radiation exposure thus enabling studies to be performed repeatedly. These short half-lives also require that the radionuclides be produced on site with a particle accelerator known as a cyclotron.

Radio nuclide	Half Life (min)	Range in Water (mm)	Maximum Positron Energy (MeV)	Reaction	Labelled Compound	Compound Application
^{11}C	20.4	1.7	0.97	$^{14}B(p,\alpha)^{11}C$	^{11}CO	cerebral blood volume
					$^{11}CH_3I$	Methionine, protein synthesis
^{13}N	9.96	2	1.19	$^{12}C(d,n)^{13}N$	NH_3	organ perfusion, metabolism
					^{13}N-amino acids	amino acid metabolism
^{15}O	2.07	2.7	1.7	$^{14}N(d,n)^{15}O$	$H_2{}^{15}O$ $C^{15}O$	cerebral blood flow
					$C^{15}O_2$	cerebral blood flow estimation
					$^{15}O_2$	oxygen consumption
^{18}F	109.7	1.4	0.64	$^{18}O(p,n)^{18}F$	fluoro-deoxyglucose (FDG)	glucose metabolism
					fluoro-dopa	ligand-receptors studies

Table 1 Radioisotopes used and their characteristics [3, 4]

2. Photon Interactions

Once positron annihilation occurs, the emitted photons can interact with the subject's body through various interactions. These include, in order of importance, Compton scattering, Rayleigh scattering and the photoelectric effect. Although 511 keV photon interactions in tissue ($Z \approx 8$ for biological materials) are dominated by Compton scattering (Figure 2) all interactions will be described here since they all cause problems for detection of the annihilation location.

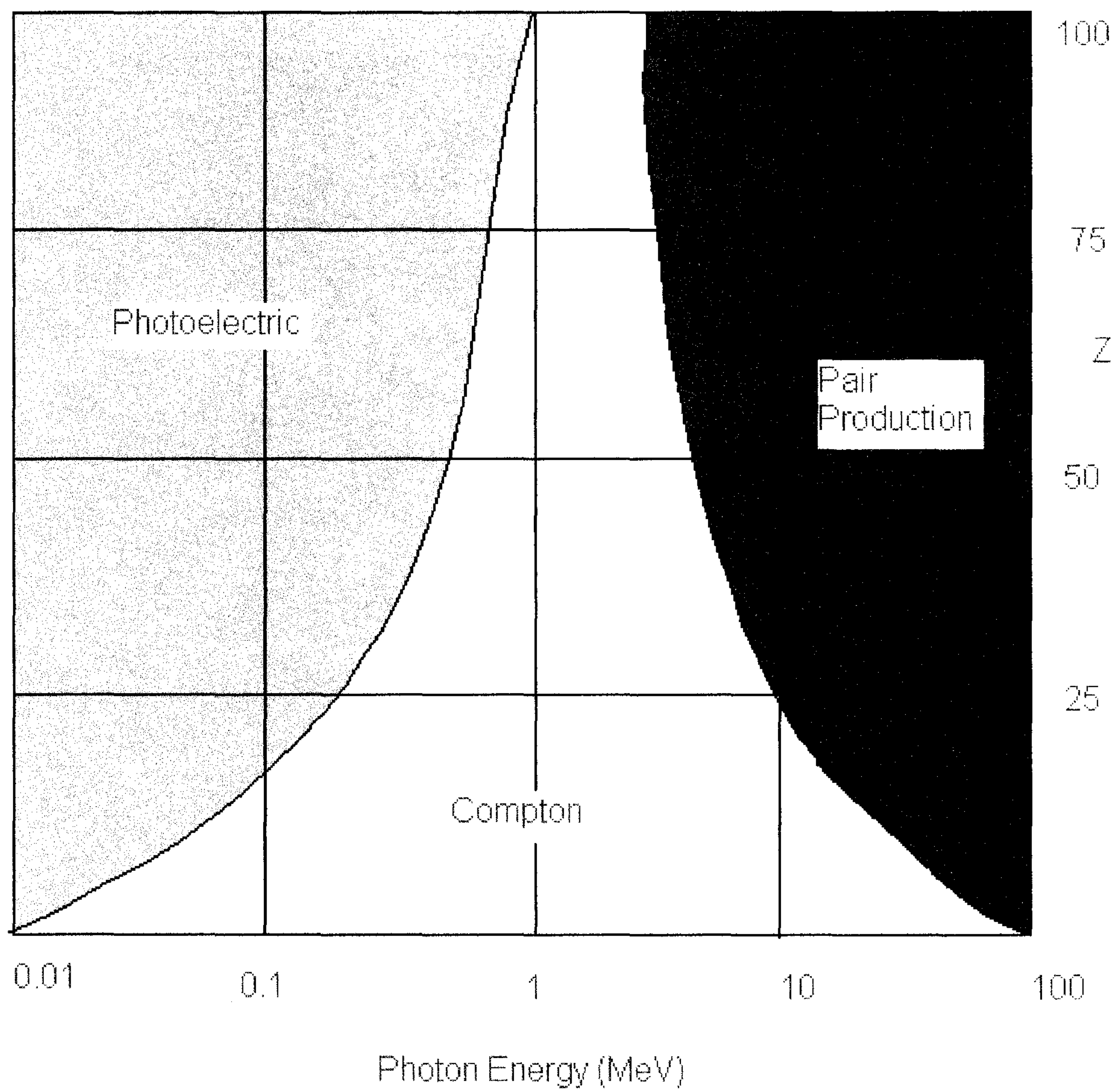

Figure 2 Interactions distribution

Compton Process

In Compton interactions a photon interacts with a free electron which results in the photon being scattered through an angle θ and the electron being ejected as illustrated on the Figure 3.

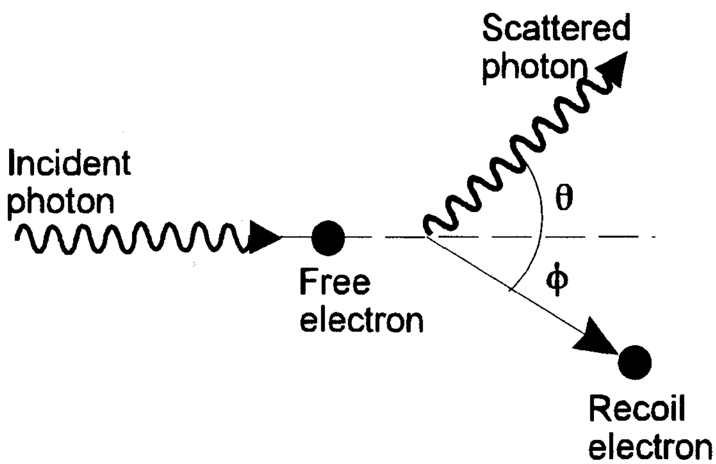

Figure 3 Compton scattering

The scattered photon energy is given by [5]:

$h\nu' = h\nu/[1+\epsilon(1-\cos\theta)]$ with $\epsilon = h\nu/(m_o c^2)$

where $h\nu$ is the incident photon energy, $h\nu'$ is the scattered photon energy and m_o is the electron mass.

Photoelectric Effect

During the photoelectric effect a photon disappears after a collision with an atom, which absorbs all its energy resulting in the ejection of what is called a photoelectron. This photoelectron has the energy of the incident photon less the binding energy. This process occurs mainly at low energies and likelihood increases at high atomic number.

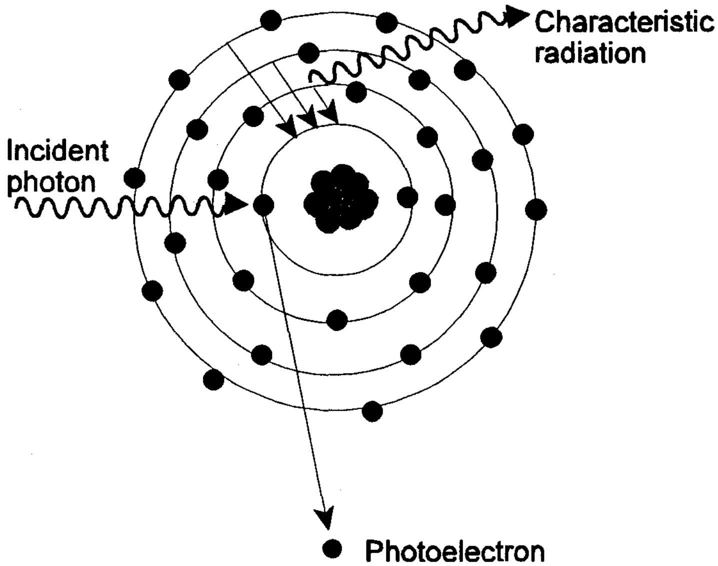

Figure 4 The photoelectric effect

Rayleigh Scattering

Rayleigh scattering occurs at low energies in materials with large atomic number (Z) values (not the case of tissue). In this process photons are scattered by bound electrons through an elastic process.

3. Annihilation Detection

In order to determine the location of the radionuclides in the body PET has a ring of detectors that are used for detection of annihilation photons. As previously stated, positron annihilation results in the emission of two γ-rays. These photons are emitted at 180 degrees to one another thus, with the help of a coincident circuit, two detectors in the detector ring will receive two signals at the 'same time'. From these signals one can locate the line of response formed by the two detectors on which the annihilation occurred. The number of counts recorded along each line of response connecting two detectors would be proportional to the activity along that line if there were no attenuation.

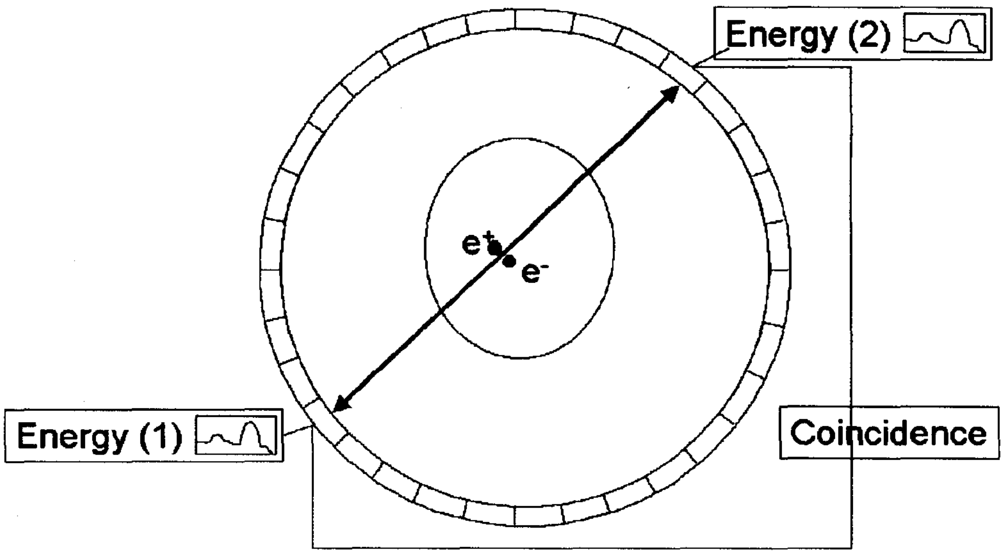

Figure 5 Annihilation detection

All this information is then stored in a sinogram: a histogram in two dimensions with the distance on the x-axis and the angle between a horizontal line and the line of response on the y-axis. Each row in the sinogram gives a projection through the object at a particular angle. If projections from all around the object are available, a tomographic cross-section can be reconstructed using CT methods.

II. COMPONENTS OF A PET SCANNER

A whole body PET scanner (CTI HR$^+$) is composed of four rings of detectors each made up of 80 blocks of 64 detectors each for a total number of crystals 4×80×64. Each block detector consists of a solid scintillator crystal cut with deep channels which are filled with white epoxy to prevent light spreading. Each crystal is then coupled to four PMTs.

1. Detectors

Crystals

Scintillation crystals commonly used in PET detectors include thallium doped sodium iodide (NaI), bismuth germanate (BGO, chemical formula: $Bi_4Ge_3O_{12}$) and cesium doped lutetium oxyorthosilicate (LSO, chemical formula: Lu_2SiO_5). These crystals all possess the property of changing gamma rays into light thanks to energy transfer during Compton or photoelectric interactions. The most important features of BGO and LSO crystals are displayed in Table 2.

Table 2. Properties of commonly used scintillators in PET [6, 7, 8]

Property / Scintillator		BGO	LSO
Relative light output		15	75
Decay constant (nsec)		300	40
Index of refraction		2.15	1.82
Density (g / cc)		7.13	7.4
Effective atomic number		75	66
Singles efficiency at 511 keV	10 mm thick	62 %	58 %
	25 mm thick	91 %	89 %
Coincidence efficiency at 511 keV	10 mm thick	38.4 %	33.6 %
	25 mm thick	82.8 %	79.2 %

A scintillation material requires several properties in order to be used as a detector. Detector crystals must be able to convert the kinetic energy of charged particles into detectable light with high scintillation efficiency, must be transparent to the wavelength of their own emissions, have short induced luminescence decay times so that fast signal pulses can be generated, have indices of refraction near that of glass in order to permit high transmission efficiency of scintillation light to a photomultiplier tube and finally the light yield should be proportional to the energy deposited. For this last reason, photoelectric effect should be the dominant interaction in the crystal so that all the energy of the incident photon is absorbed and thus detected. Unfortunately this is not the case for any currently available scintillator at 511 keV (BGO 45%).

Illustration of principles of scintillator crystals

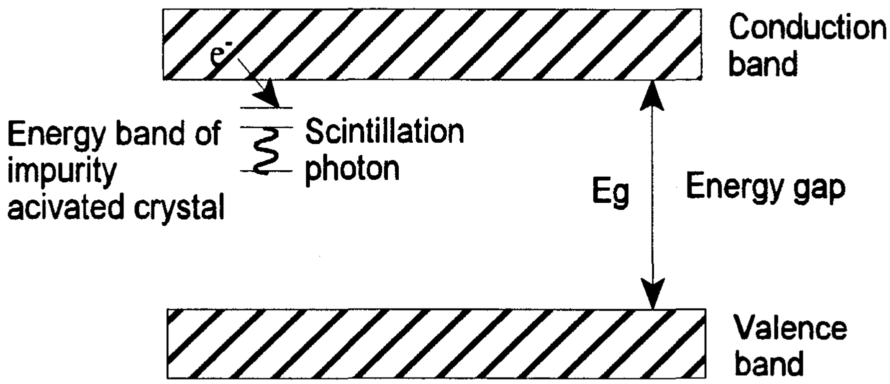

Figure 6 Scintillator crystals

Figure 6 illustrates how photons lose energy interacting with scintillator crystals. This energy is used by free electrons in the valence band to reach the conduction band by overcoming the energy gap. Once the electron is in the conduction band it falls back to the valance band via energy bands created by impurities introduced in the crystals. The energy lost in transitions to and from these intermediate bands results in the emission of visible light.

Photomultiplier tube

A photomultiplier tube (PMT) is a sensitive device for measuring photon counts. In PET each of the detection crystals is connected to a PMT that detects the visible light emitted through the scintillation process. The scintillation light enters the phototube through an entrance window where it strikes a photocathode that emits free photoelectrons into the vacuum in a number proportional to the number of photons striking it. The conversion efficiency varies with the wavelength of the incident light. Typically the relationship between the two is given by a spectral response graph and one needs to choose a PMT according to these characteristics.

The photoelectrons emitted are then attracted to the first in a series of dynodes of increasing potential. These dynodes emit about three to five times the number of electrons striking them which results in electron multiplication. Typically PMTs contain 8 to 19 stages of such dynodes which results in a gain of approximately 10^6 [9]. Finally the anode collects all the electrons as an output signal and sends them to the phototube's output circuit. The output circuit is designed to give a voltage pulse whose height is exactly proportional to the total number of electrons collected by the anode.

Figure 7 PMT design

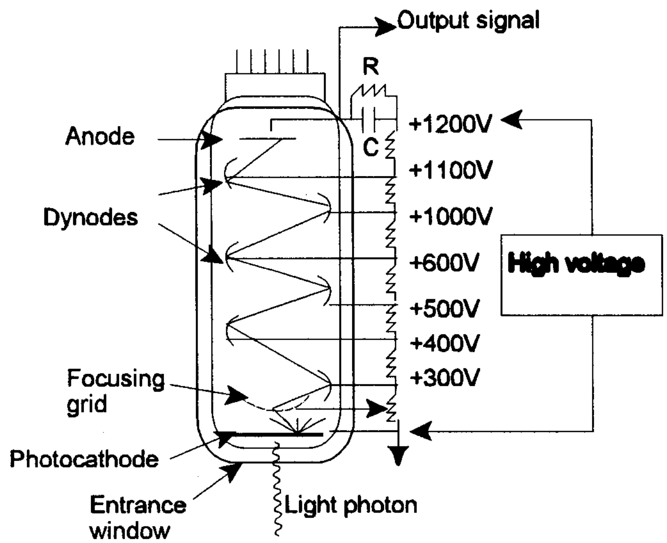

Scintillation counting

All radiation measurements require the determination of two parameters: the number of particles detected and the energy of each particle. As previously mentioned, radiation entering a scintillator crystal results in the production of light flashes where the number of light flashes is proportional to the energy deposited in the scintillator. The PMT which analyses these light flashes must be capable of producing a signal proportional to the energy as well as distinguishing between consecutive light pulses that correspond to different particles and additive light pulses representative of the energy of one radiation. As such, another important parameter for a PMT is the quantum efficiency which characterizes the pulse height resolution.

2.Collimators

Collimators are used in PET to direct the annihilation photons in the scanning field of view. Two types of collimators are used in modern multi-slice PET scanners: thick lead rings for the definition of the external axial field of view and thin "septa" made of lead or tungsten rings (1-5 mm) for the definition of the individual imaging planes. The septa are used to define the slices during 2D acquisition and are retracted during 3D scans.

3. Signal Processing

The PMTs are coupled to the scintillator crystal in a configuration known as "Anger logic" as a reference to the Anger camera used in nuclear medicine. The PMTs are commonly referred to as A, B, C, and D and cover the crystal as shown in Figure 8.

Figure 8 PMTs arrangement

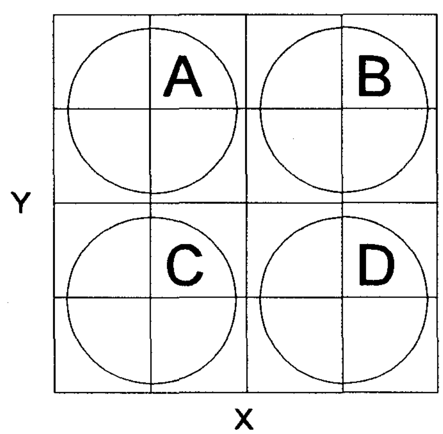

The estimation of the position and the energy of the annihilated photons is then given by the following equations:

$$X=\frac{[A-B]+[D-C]}{A+B+C+D} \qquad Y=\frac{[C-A]+[D-B]}{A+B+C+D} \qquad E=A+B+C+D$$

In our animal PET scanner (ANIPET) [10] these three signals are digitized with an eight bit analog to digital converter (ADC) when it is triggered by the coincident module (usually, in PET scanners, each event is digitized and only coincident events are processed). In order to accept a count and store the photon's position the energy has to be in-between the upper and lower discriminator settings.

4. Coincidence Detection

A coincidence system determines when two events occur within a certain fixed time period. In practice it is not possible to analyse coincidence events with 100% accuracy due to uncertainties associated with the statistical nature of the process (see Poisson statistic paragraph). Each coincident photon pair detected corresponds to one count which is stored in the sinogram. The signal coming from each photon has a maximum allowable time difference called the coincidence resolving time (commonly represented by the symbol τ). Typical resolving times are 10 nanoseconds or less for a range of energy from 0.1 to 1 MeV [11]. Shorter resolving times are possible with plastic scintillators which have very fast light decay. In PET, the time window is typically in the range of 8-16 ns for whole body scanners due to the relatively "slow" scintillation light decay, and the time taken for the photon to cross the field of view.

5. Image Formation

All counts coming from the annihilation photons are stored in memory arrays called sinograms as mentioned earlier. This format of data storage is the most suitable for direct use by standard image reconstruction programs. Figure 9 represents an annihilation, A, occurring inside the scanner where P and Q are the detectors in coincidence. The centre of the detector ring is represented by O while H is the point on PQ that perpendicularly connects to O.

Now we have:

$\text{ang}(P) = 2\pi P / N$

$\text{ang}(Q) = 2\pi Q / N$

$\beta = \pi / N \times (P+Q)$

where N is the total number of detectors and P and Q are the detector numbers.

If we now assign:

$[OH] = s$, $[OA] = d$, and $[OP] = R$ (radius)

Figure 9 Sinogram composition

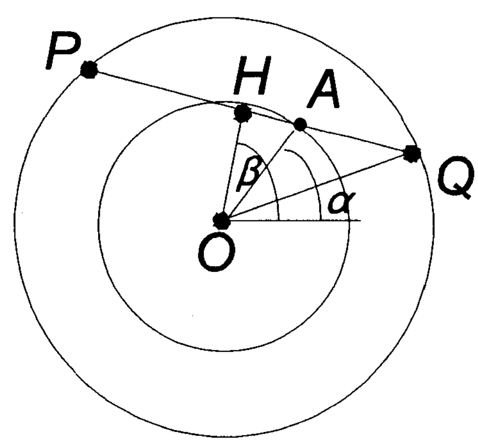

then

$s = R \cos 2\pi(P-Q) / N$

and thus $s = d \cos(\beta-\alpha)$ where α is the angle that characterises point A.

The horizontal axis of the sinogram represents the distance from chords like PQ to the centre of the scanner, s, and the vertical coordinate represents the angle of the line of response, β.

The advantage of this set up is that each line on the horizontal row of the sinogram represents a projection of the image at the angle β and the reconstruction program uses projections at different angles. An illustration of a sinogram is shown in Figures 10, 11, and later in this thesis, in Figure 16.

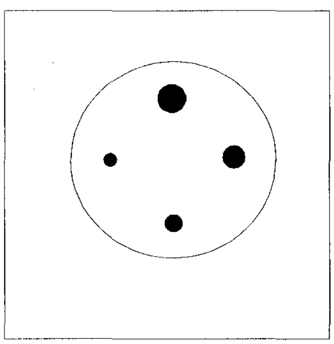

Figure 10 Cylinder used for the sinogram on Figure 11

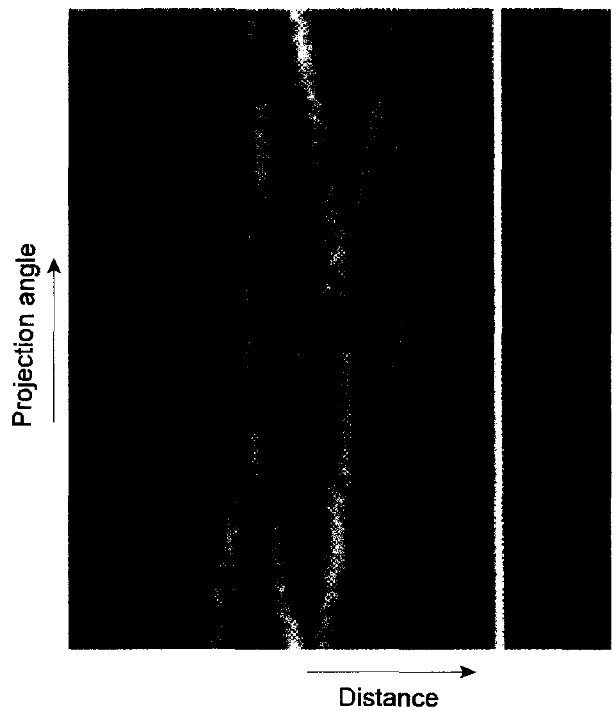

Figure 11 Sinogram picture showing several point sources in a cylinder

III. RESOLUTION IN PET

Resolution in PET is primarily dependent on two parameters: the positron range and the angular distribution of the annihilation photons.

1. Positron Range

An emitted positron does not annihilate immediately but instead travels a certain distance in the medium before losing its kinetic energy. This distance is typically a few millimetres in tissue. This causes spatial resolution distortions since the annihilation occurs distant to the actual radionuclide location.

Figure 12 Positron range [2]

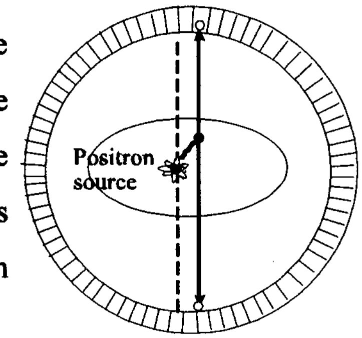

--- Real annihilation position

—— Line of response assumed by PET

2. Angular Distribution of Annihilation Photons

The angular distribution problem occurs due to the fact that annihilation photons are not emitted with precisely 180 degrees between them. In practice there is an angular deviation of about 0.5 degrees for all materials [12]. The loss in resolution resulting from this effect depends on the coincidence detector separation. Typically for a 50 cm detector ring radius the error due to the angular distribution of annihilation photons is $\pm$ 2.2 mm (500 mm $\times$ $\tan\{0.25°\}$).

Figure 13 Angular distribution of annihilation photons [2]

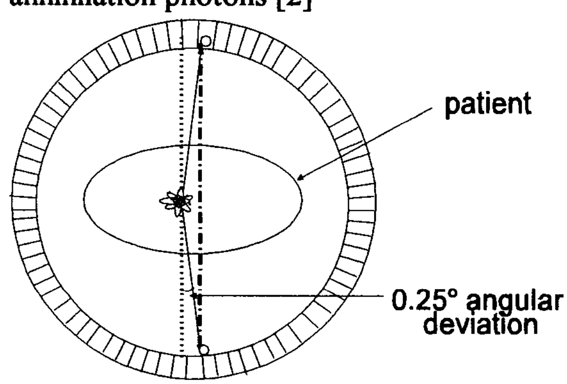

·········· correct line of response

-·-·- incorrect line of response

3. Practical Limits

There are various practical limits which reduce resolution in PET scans. These include the limited activity allowed per scan and several instrumentation limitations such as the detector size, the coupling efficiency between the PMTs and the crystals and various sources of noise.

V. SOURCES OF NOISE IN PET

As in all imaging techniques, the image quality in PET is highly noise dependent. There are several sources which introduce noise in PET images.

1. Poisson Distribution

Poisson distribution involves the statistics of radiation counting, statistical noise is common for all techniques that involve counting photons. Since radioactive decay from the activity inside the patient is random if there are N counts acquired per unit time, the uncertainty due to Poisson statistics will correspond to $\sqrt{N}$.

2. Scattered Events

Scattered event contamination is caused by annihilation photons that have been scattered inside the subject before reaching the detectors. These events degrade the image quality and reduce the accuracy of quantitative measurements [13]. The line of response (LOR) identifying these photons is thus not the correct one. To overcome scatter problems each projection is convolved with a smoothing function which represents an estimation of the scattering probability. This estimation is then subtracted from the counts obtained.

Figure 14 Scatter and random events [2]

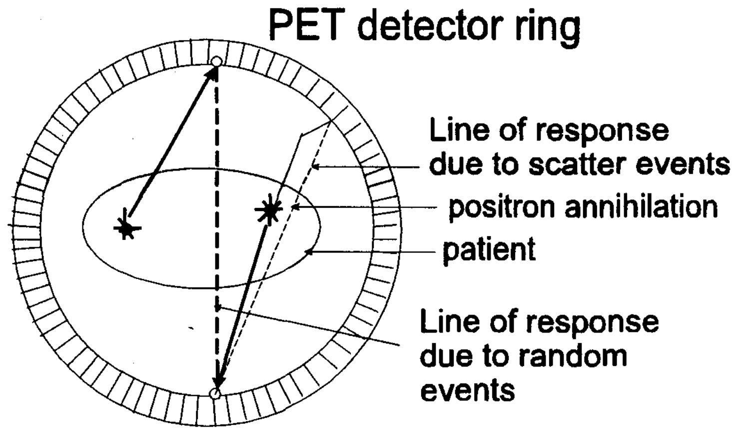

3. Random Events

Random event noise comes about due to the coincidence set up mandatory in PET. Events from two different annihilations can occur at the same time and be identified as a LOR. The contamination from random counts occurring at the same time increases with the coincidence time window τ. The count rate R of a detector pair is given by:

$R = 2\,\tau\,D_1\,D_2$.

where D_1 and D_2 are the individual detector count rates.

Correction for random events is performed by estimating the random event contribution and subtracting it from each point in the sinogram. The estimation is performed by using two timing windows, one with no delay and the other with a 20 ns delay. The signal from the window with the 20 ns delay should contain only random events whereas the signal from the window with no delay has both true and random events. The difference between the two is then taken as the random event contribution estimation.

4. Dead Time

In all detector systems there is a minimum amount of time that must separate two events in order that they are distinguished from one another. This time is called the dead time. If a pulse arrives at the detector during the dead time, it is not recorded. The dead time increases with the count-rate and the detector surface thus making the detector as small as possible is a major consideration in PET design.

5. Out of Field Counts

As explained later, PET scanners can easily acquire data in two or three dimensions. In the 2D method, the detection is done slice by slice. As a result counts can be detected from annihilations taking place outside of the slice of interest. Septa are thus used to protect each detector from receiving counts outside of the slice field. In 3D studies septa cannot be used and image quality decreases as the out of field of view contamination increases. These out of field counts contribute to the random events noise.

6. Noise From Attenuation Correction

Noise from attenuation correction is very significant in PET and will be discussed in the transmission / emission scans chapter.

CHAPTER 2

GENERAL PRINCIPLES OF TRANSMISSION AND EMISSIONS SCANS

I. INTRODUCTION TO THE ATTENUATION CORRECTION MECHANISM

Transmission scans are used to measure the attenuation of annihilation photons in the body of the patient being scanned. When traversing the longest attenuation paths through a head section only one pair of photons in seven emerges unscattered. The mass attenuation coefficient of water (tissue equivalent) at 511 keV is 0.097 cm^{-1} [5] which means that, for a big patient in which this path can be as large as 40 cm for a body scan, the attenuation can cause the transmitted photons to be reduced by a factor of almost 100. An example of the attenuation effect on a circular phantom is shown in Figures 15 and 16.

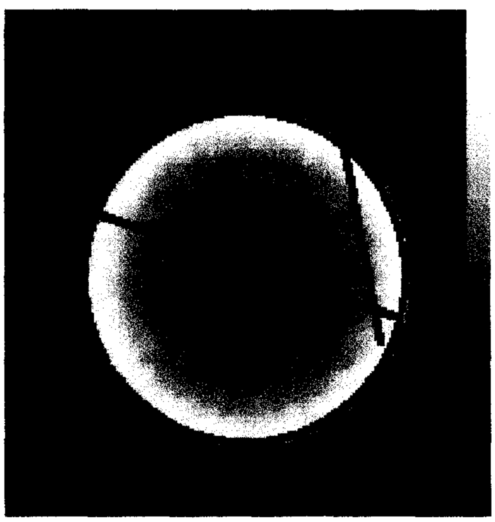

Figure 15 Emission scan without attenuation correction

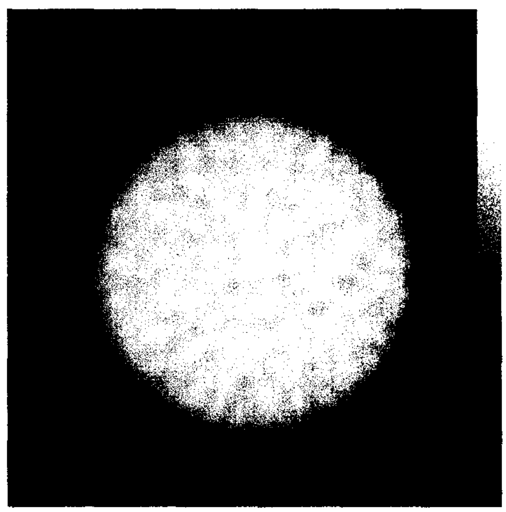

Figure 16 Emission scan with attenuation correction

As illustrated above, the corrected image is more uniform indicating the importance of attenuation compensation in quantitative PET imaging.

1. A historic overview of transmission scans

Several techniques have been proposed to correct for attenuation in PET. The first technique ever used was an analytic correction purposed by Huang [14, 15] in a study on the effects of inaccurate attenuation correction in PET. The first measurement of attenuation was performed by Derenzo [16] in 1979 using a ring of positron sources surrounding a patient being scanned. A major problem of this technique was the contamination by random and scatter events. To overcome this problem Carroll *et al.* [17] proposed the use of a small concentrated source rotating around the body section with a selection of events collinear with the source to reduce the contamination. Many improvements have been proposed and studied such as the possibility of post injection transmission scans by Kubler [18] or simultaneous emission and transmission scans by Thompson and Ranger [19]. Presently many possibilities for performing transmission scans exist as will be described in detail shortly.

2. Use of external sources

The annihilation photons (511 keV) from positron emitting isotopes are attenuated while exiting the body of the patient. In order to account for this attenuation, a transmission scan yielding the extent of attenuation is required. In Figure 17, the positron annihilation is represented by the black dot. This annihilation creates two gamma rays travelling through the distances L_1 and L_2. The probability that both photons reach the detectors is given by:

$$P = P_1 \times P_2 = e_{L1}^{-\int \mu(x)dx} \times e_{L2}^{-\int \mu(x)dx} = e_{L}^{-\int \mu(x)dx} \qquad (1)$$

where μ is a two-dimension mass absorption coefficient.

Figure 17 Attenuation correction

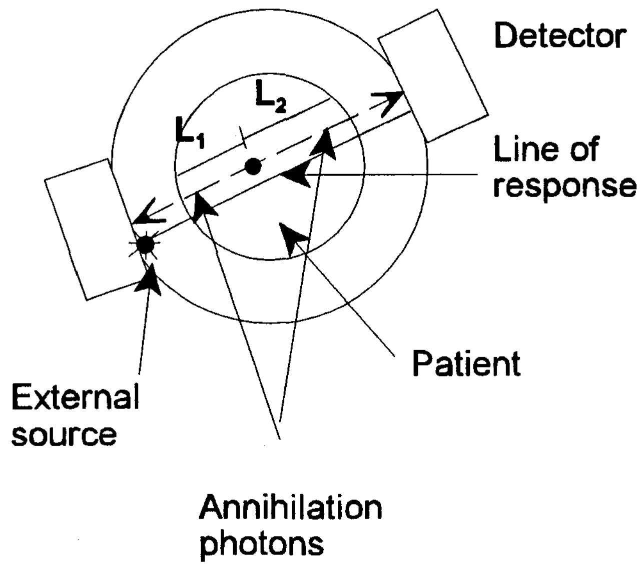

As indicated by Equation 1, the attenuation along the line of response is independent on where the annihilation takes place. As such, two annihilation photons emitted at 180 degrees will have the same probability of detection whether they originate in an external source or from within the patient section. Usually one or several external point sources rotating around the patient are used for transmission scans.

3. Blank scan

In order to take into account the detectors' efficiency, blank scans are typically performed on PET scanners every morning. A blank scan consists of recording a scan of the external sources without a patient present thus representing the unattenuated case.

The blank scan is used to calculate an attenuation correction factor (ACF) which attempts to cancel out the photon attenuation effect. The ACF is the ratio of the measured counts with and without the attenuating object. The ACFs form a sinogram which is a representation organized by transverse chord positions (horizontal) and chord angles (vertical) whose elements express the amount of attenuation for the detector pair d. The data forms a sine wave in the vertical direction as illustrated in Figure 18.

The attenuation pre-correction is carried out as the multiplication of the emission sinogram count by the corresponding ACF.

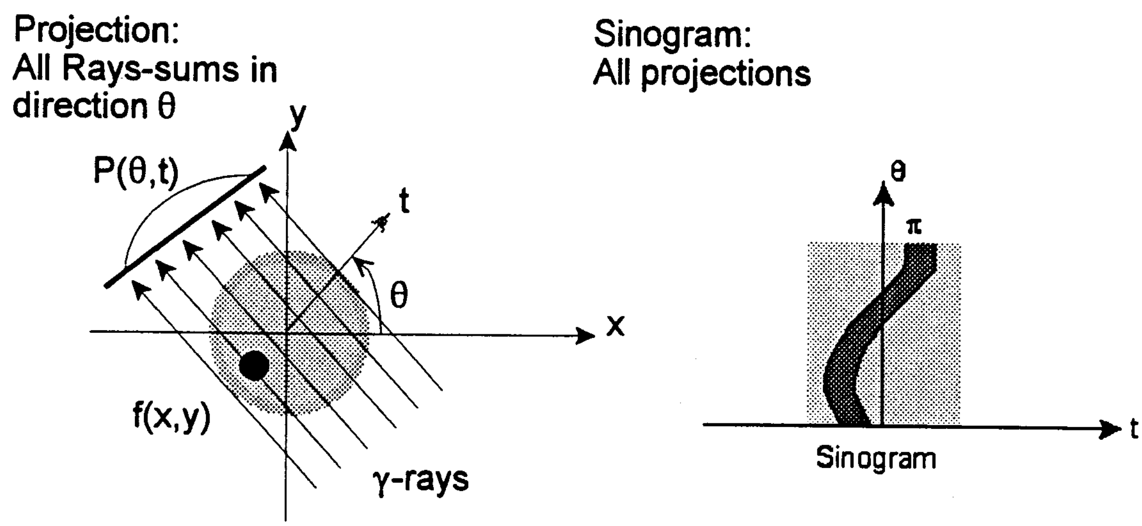

II. PET EMISSION IMAGING MODES

PET scanners acquire data through the use of one of two different modes: two-dimensional mode (2D) or three-dimensional mode (3D). Both of these techniques have inherent advantages and disadvantages. The most important difference between these modes is the presence of interplane septa (thin lead or tungsten annuli) in the 2D mode in order to reduce random and scattered coincidences. While achieving this goal the septa also eliminate coincidence lines of response between pairs of detectors that are more than three to five rings apart.

1. 2D PET imaging

As mentioned previously, the 2D imaging mode requires the use of septa between the individual sets of crystals. Septa are designed to provide maximum shielding from out of plane scatter while still allowing coincidences between adjacent rings. They also serve to reduce the singles and random rate for a given activity within the field of view and to shield the detectors from activity outside the field of view. PET cameras in this mode operate with coincidence lines of response restricted to detectors lying either within the same ring (direct planes) or within adjacent rings (cross planes). In this case the camera images a three-dimensional volume as a set of independent two-dimensional slices as illustrated in Figure 19.

Figure 19 2D PET imaging

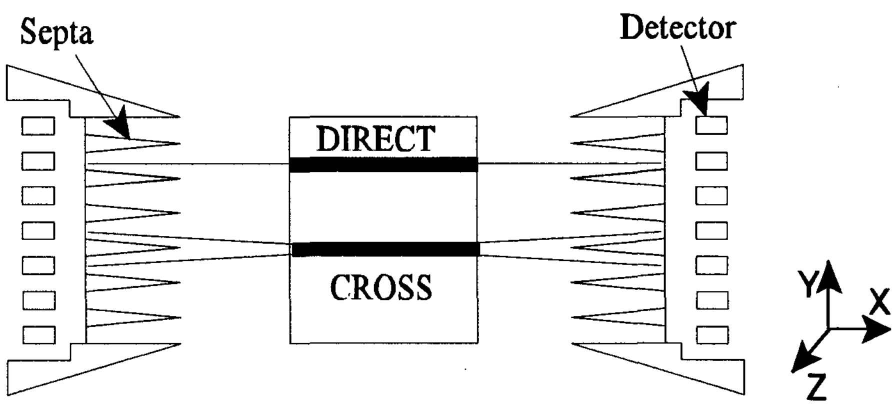

As a result 2D images acquired using this mode are well defined and almost insensitive to scattered γ-rays in the plane defined by septa (xy plane) unless the γ-rays are scattered with a very large angle in the yz plane as shown on Figure 19. In that case the γ-rays can be scattered through quite a large angle and still be detected.

2. 3D PET imaging

Thanks to the septa retraction available on recent PET scanners, 3D acquisition is now possible as shown in Figure 20. In this mode each detector can detect and form LORs with detectors from different rings. Although 3D PET acquisition increases the number of LORs for reconstruction, septa removal has a number of important consequences. The singles rate from activity both inside and outside the field of view increases and results in a higher random rate and potential dead time problems. The axial resolution is slightly degraded due to oblique penetration in the detectors and assumptions made which ignore the obliquity of these rays.

Finally, the most important problem comes from the sensitivity of the scanner to scattered rays. This sensitivity can increase by up to 20 times thus inducing contrast loss.

Figure 20 3D PET imaging with septa removed

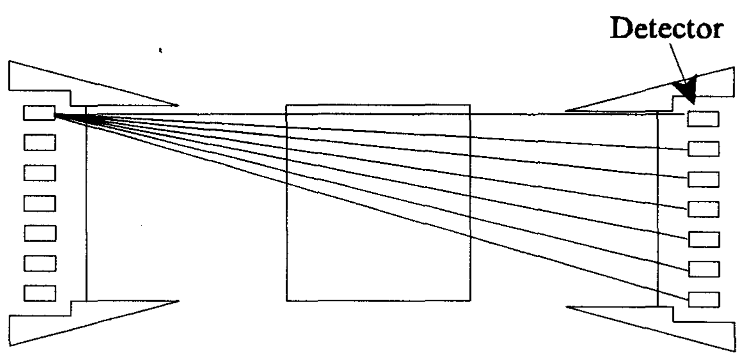

III. CONVENTIONAL TRANSMISSION SCANS

1.Orbiting rod coincident transmission scans

Before the introduction of orbiting sources [17] attenuation correction values were calculated using simple geometric shapes to approximate the attenuation medium. This method was not ideal for all applications (mainly used in brain imaging) and the magnitude of the error in quantization of activity concentration was shown to be significant [14]. Body imaging required the use of transmission scans due to the wide range of attenuation coefficients in going through the heart, lungs and ribs. Positron emitting isotopes were first used for transmission scans by Derenzo *et al.* [16]. The authors describe a stationary positron tomograph. Their method of implementing the transmission correction employs a ring or a hoop source of annihilation radiation. The system consisted of a hollow hoop shaped container filled with ^{68}Ge. An illustration of the decay scheme is shown in Figure 21.

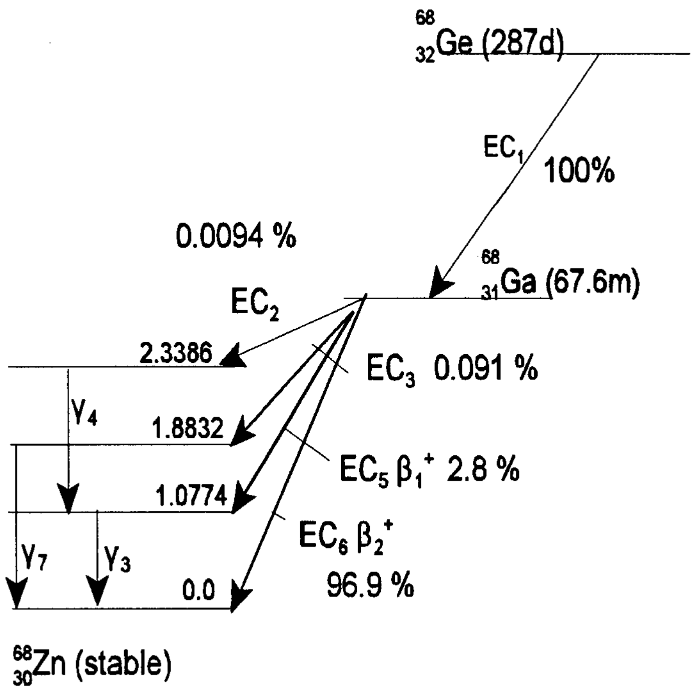

Figure 21 ^{68}Ge decay scheme

This design was implemented on an early PET scanner which consisted of 280 closely-packed rectangular NaI (Tl) crystals, lightpipe, and phototubes. In this communication Derenzo mentioned the possible dead time problems of moving line source transmission measurements. These problems occur whether or not coincidence mode is used even if the selection of events is limited to those that pass through the source.

The possibility of using rotating line sources (Figure 22A) instead of a ring source for PET transmission measurements was first introduced in 1981 by Derenzo *et al.* [16]. It has since been incorporated in several commercial PET systems. An alternative to Derenzo's design was introduced by Carroll *et al.* [17] in a detailed study using a small concentrated source rotating around the body section (orbiting rod source). Derenzo's hoop source (Figure 22B) had to move from one slice to another in order to obtain different axial transmission scans on multi-slice scanners. The orbiting rod source (Figure 22C) overcomes this problem and has the advantage of a known source position at any time which can be exploited to reject accidental coincidence events. The authors applied a masking algorithm to select the chords within a given acceptance angle and they particularly stressed the reduction of random events in the transmission data. An increased contrast in transmission images which arises from scatter and random rejection following a suggestion by Carroll [17] has been reported by Thompson *et al.* [20]. The authors use the basic principle that the annihilation photons are co-linear and thus the position of the source and detectors which record the gamma rays at any time permit masking of the events for which the co-linearity condition is violated.

In all the preliminary studies described above the objects being scanned happen to never exceed a diameter of 20 cm. For these small objects the scatter content is on the order of 10% to 20% in both transmission and emission scans. Consequently the corrections were relatively small. Furthermore, the scatter in ring source transmission measurements tended to compensate for the scatter in the emission images. Kubler [18] investigated the influence of scatter contamination in the transmission data on the attenuation correction in large objects. She concluded that the attenuation corrections using ring-shaped transmission sources did not work satisfactorily in whole-body PET studies and further investigations were needed.

Presently orbiting rod coincident techniques are the most commonly used transmission scans. Several sources (usually ^{68}Ge rods with windowing) are placed as close as practical to the inner surface of the septa and are rotated around the patient as shown on Figure 22C. Scattered γ-ray detections are low due to inter-plane septa and noise rejection can be implemented using windowing or masking as first reported by Carroll *et al.* [17]. The major problem encountered using these techniques is the high counting losses for the detectors close to the transmission sources (the near detectors in Figure 22C) thus resulting in low counting statistics.

Figure 22 Evolution of the attenuation correction

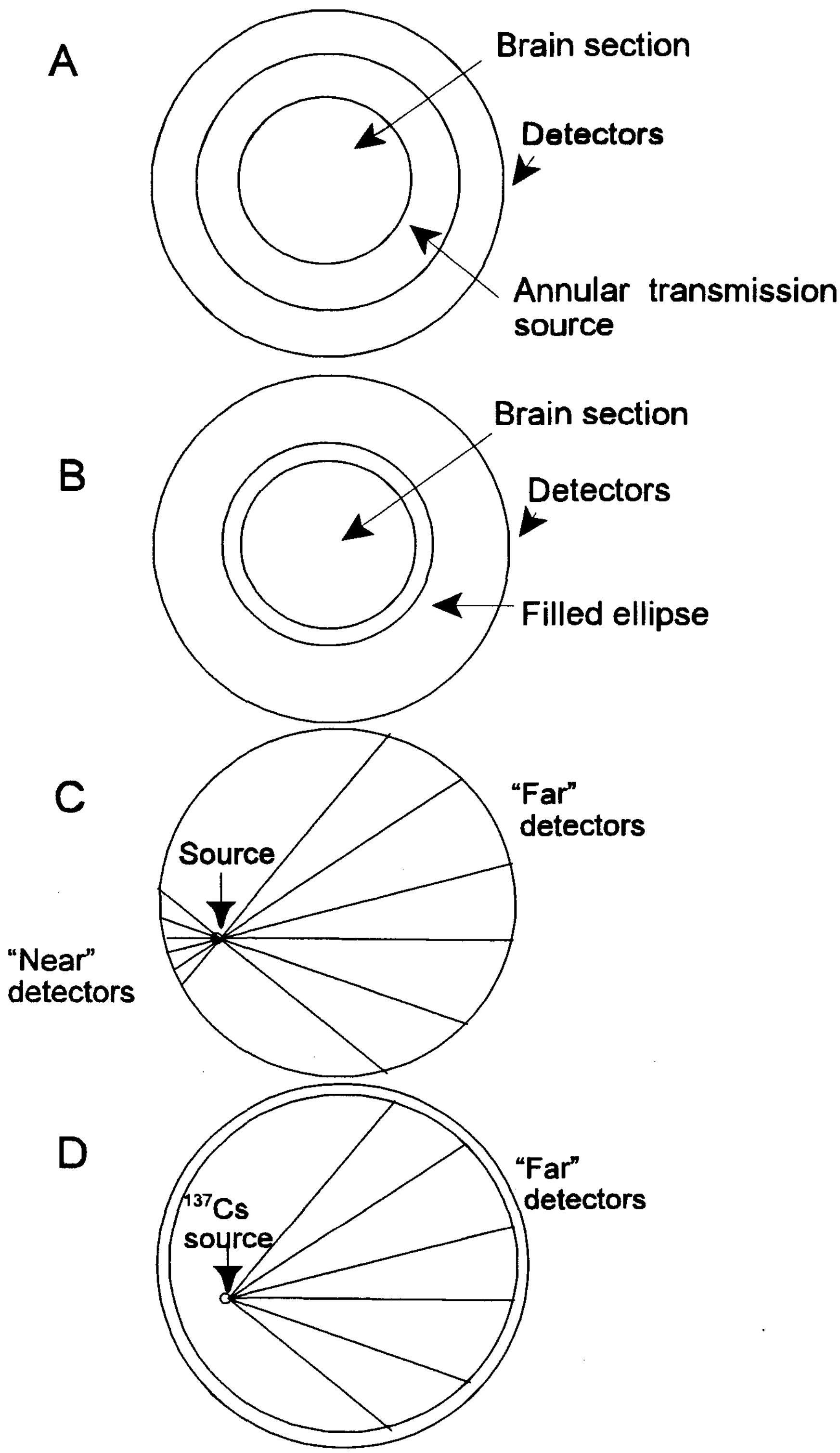

2. Single-photon orbiting transmission scans

Single-photon orbiting transmission scans use single-photon emitting isotopes (^{137}Cs) for transmission scans as shown in Figure 22D. The application of a single-photon source for transmission measurements was first introduced in Single Photon Emission Computed Tomography (SPECT) studies by Bailey *et al.* [23]. This group used two radionuclides with different energies for emission and transmission scans distinguished by pulse height energy discrimination. This method had the advantage of being able to perform emission and transmission scans at the same time thus avoiding problems associated with repositioning and misalignment as well as reducing the scan time by a factor of two. A single-photon source was first introduced in PET as a transmission source by deKemp and Nahamias [24] who used a rod positron-emitting source with singles triggering and septa collimations. The main advantage of using a single-photon transmission source over the coincidence technique is a dramatically increased count rate (as high as a factor of 7). A ^{137}Cs point source was first reported as a transmission source by Karp *et al.* [25] and Yu and Nahmias [26] in 1995. The use of ^{137}Cs was motivated by its long half life, approximately 40 times longer than ^{68}Ge, and its relatively low cost. ^{137}Cs emits two beta particles of 1.176 MeV and 0.514 MeV, a mono energetic gamma ray of 662 keV and barium x-rays as shown in its decay scheme in Figure 23.

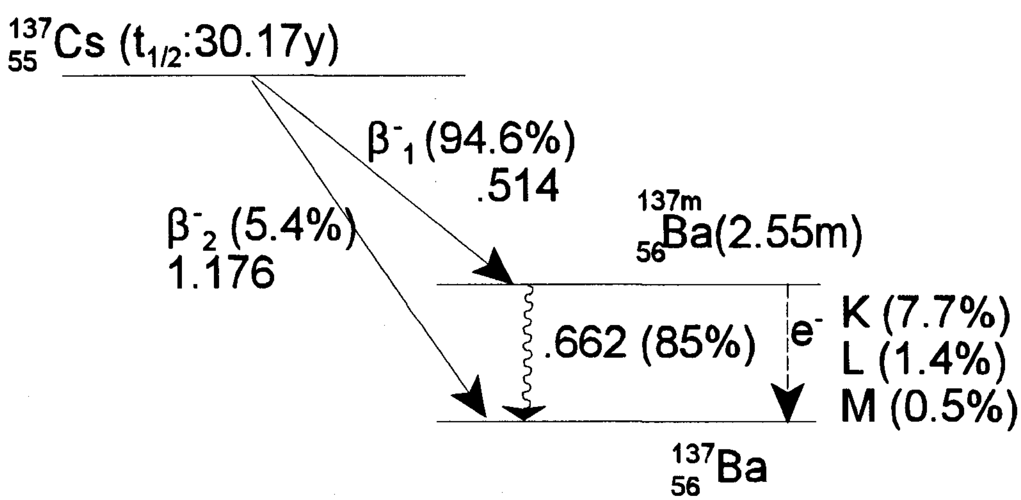

Figure 23 137-Cesium decay scheme

The barium energies are all below 40 keV and will be excluded by the photopeak window low-level discriminator while seven millimetres of Perspex around the source were used as shielding against the beta particles emitted. These beta particles produced bremsstrahlung radiation in Perspex that could be neglected. Karp, Yu and Nahmias [25, 26] demonstrated that the image noise in transmission scans is substantially reduced with a ^{137}Cs transmission source since the singles count rates are much higher than the coincident count rates. ^{137}Cs as a point source also allowed for short acquisition times (reported to be about 10 times faster than using orbiting rod sources) [25].

The positron-emitting source strength is usually limited by the count rate of the "near" detectors, which in turn limit the coincident count rate. In the "singles" method only the "far" detectors determine the saturation of the system so a stronger source can be used resulting in a higher event rate. Since 662 keV γ-rays are being used for transmission scanning, measured attenuation coefficients will be 10% lower than those from the 511 keV γ-rays of the emission data. Scaling of the measured attenuation factors to make them applicable to the emission data is thus necessitated. Several scaling methods are currently under study including segmentation, emission contamination subtraction with scaling and some hybrid techniques which will be further discussed later [28, 29]. Another disadvantage of using ^{137}Cs is the reduction in contrast between cortical bone and soft tissue. Although the use of 662 keV γ-rays instead of 511 keV γ-rays results in a loss of approximately 9%, the ratio of mass attenuation in water to bone only deviates by 0.5% as reported by Yu and Nahamias which allows for simple extrapolation of the linear attenuation coefficients.

Finally a new approach has been proposed by Jones *et al.* [30, 31] using a collimated coincidence point source with a dedicated reference detector. In this case the point source is a sealed ^{68}Ge source with an LSO crystal coupled to a PMT in order to detect the annihilation gamma rays. As each dedicated LSO crystal is placed close to the point source and isolated by collimation, most of the annihilation photons have a known origin avoiding the need for accurate energy discrimination and long pulse shaping time. Jones *et al.* are also implementing a 3D approach of simultaneous transmission and emission scans using this method. The faster scintillator and lack of block decoding give a pulse processing time reduced from 315 ns (with BGO) to 120 ns.

3. CT or MRI correction attenuation

An alternative technique for attenuation correction would be to use attenuation values determined from a CT or magnetic resonance imaging (MRI) scan from the same body section as the PET scan. In order to have the same attenuation as PET, tissue segmentation must be carried out based on the contrast mechanism in MRI or attenuation at lower energies with CT. Major problems with these techniques include the reproduction of the patient position between these different modalities as well as the probable thickness acquisition and shape variability from one scanner to another. Finally one could use a new generation CT-PET scanner [32] but this would be an expensive solution.

4. Problems due to post-injection attenuation scans

All the methods described above assume that there is no activity in the patient (that all transmission scans are performed before tracer administration). Unfortunately, for studies that require a long uptake period there is a significant time between transmission and emission scans. Conventional fluorodeoxyglucose (FDG) studies, for example, require at least 45 minutes. This long period of scanner time limits the throughput of the scanner and increases the likelihood of patient motion. One of the methods proposed to solve this problem is to monitor the source position as it rotates about the patient aperture and reject coincidences that do not intersect with the source position [22]. This process, called sinogram windowing, removes most scattered and random coincidences from the transmission measurements thus removing bias and reducing noise. The remaining emission counts are then removed by subtracting data obtained from the emission scan which unfortunately generates a small increase in error. This method makes simultaneous emission and transmission scans possible.

5. Simultaneous emission/transmission scans

The first simultaneous emission/transmission scan was introduced in PET by Thompson *et al.* [19]. The authors used the following principle: during the transmission scans detectors that are collinear to the rod source store transmission scans whereas other detectors can still detect the activity inside the patient. One could use this information and perform an emission scan with only the detectors that are not collinear with the source. In simultaneous emission and transmission scans there are two sinograms for each patient section. Each event is determined by look up tables if the line joining the two detectors is or is not collinear with the current position of the source. Another method proposed by Thompson *et al.* [33] was to collimate several sealed ^{68}Ge point sources, one for each slice, so that annihilation photons are shaped to the field of view fan beam. Thanks to the source geometry, the 'near' detector would be protected from emission radiations and would thus receive transmission data exclusively eliminating the error due to emission/transmission subtraction. Unfortunately, image quality using simultaneous emission and transmission scans is poor especially when scanning obese subjects or when short scanning times are used. Although the accuracy of these systems was good overall, the precision was poor due to low count-rates.

6. Noise due to attenuation correction

Since the attenuation correction from a transmission scan is the result of dividing the data in the blank scan's bins by the data from the transmission scan's bins, the noise in an attenuation correction image is very unique. When ACFs are obtained by actual measurement, statistical noise is unavoidable. This noise will increase noise levels in the reconstructed image. These problems occur in post-injection transmission scans, if the activity concentration is in a high attenuation value region. High attenuation regions result in high attenuation numbers whereas high activity concentrations result in low attenuation values. Since the high activity region would be more attenuated than others this implies that one can not see hot spots.

7. Transmission scan processing

In clinical practice, the nuclear medicine physician has to decide quite frequently whether or not measured attenuation correction is worthwhile to make an accurate diagnosis [34]. Noise from the transmission scan, as explained above, can contribute significantly to the statistical quality of the final emission image. Transmission scans give better attenuation correction but in order to have noiseless, high resolution images, long transmission scans are commonly required. Unfortunately, the length of transmission scans is an issue if one wants to scan a maximum number of patients. Long transmission scans in whole-body studies where multiple bed positions are used are often impossible. Several techniques have been developed to improve the transmission image so that no extra noise is added to the emission scan. Image segmentation methods such as those developed by Xu [35] or Riddell [36] split the image up into regions that hold some property distinct from their neighbours. An essential first step in automatic procedures for analysing the content of images lies in two main approaches: identifying regions or identifying edges (or lines). These methods have not been widely adopted yet partly because segmentation on a short transmission scan is very difficult due to the excessive noise.

IV. PET IMAGING MODES

There are several different acquisition (or emission) modes in PET.

1. Static emission scans

In order to obtain a high quality static emission image we need a generally stable activity distribution and a long counting time. Measurements of the glucose metabolism of the brain or heart using FDG tracers are typical applications of static emission scans.

2. Dynamic emission scans

Dynamic studies are performed when it is necessary to follow the activity over a long period. Only one attenuation scan is done for the whole study and it is used to correct all frames.

3. Whole-body scans

Whole body scans are the fastest growing application of PET. They are also our main interest as an attenuation correction application. Whole body studies require multiple bed positions and for every position a transmission and an emission scan must be performed. For each transmission scan the use of septa with orbiting rod sources and the re-configuration of the scanner and its electronics between emission and transmission scans add a considerable amount of time (about 2.5 min on CTI HR+) to the scan. A better and faster attenuation correction that would not require the use of septa would be a considerable improvement and would decrease the scanning time.

CHAPTER 3

OVERVIEW OF BETA-GAMMA COINCIDENCE SYSTEM

I. MOTIVATION FOR SYSTEM DEVELOPMENT

1. Introduction

We propose a different approach to the coincident point source setup used by Jones [30, 31]. Our approach uses beta-gamma coincidence and 3D acquisition to improve the quality of transmission scans. This method has the same advantages as single photon attenuation correction using ^{137}Cs without the problem of having to scale the attenuation coefficients due to the different photon energies (0.662 MeV from ^{137}Cs versus 0.511 keV from the annihilated photons). It is well known that a positron must lose an appreciable amount of its energy before annihilation with an electron can occur [37]. In our setup the energy lost by the positron is spread inside a plastic scintillator material which produces light detectable by a PMT. This PMT signal is then used to trigger an acquisition circuit and identify a line of response between the plastic scintillator and the PET detectors as shown in Figure 24.

The concept of beta-gamma coincidence was first proposed by our group in 1999 using PIN diodes to detect the positron [38]. The work presented in this thesis represents the first time beta-gamma coincidence has been attempted using plastic scintillator detectors as well as the first implementation of beta-gamma coincidence on an actual PET scanner.

Figure 24 Basic positron detection diagram

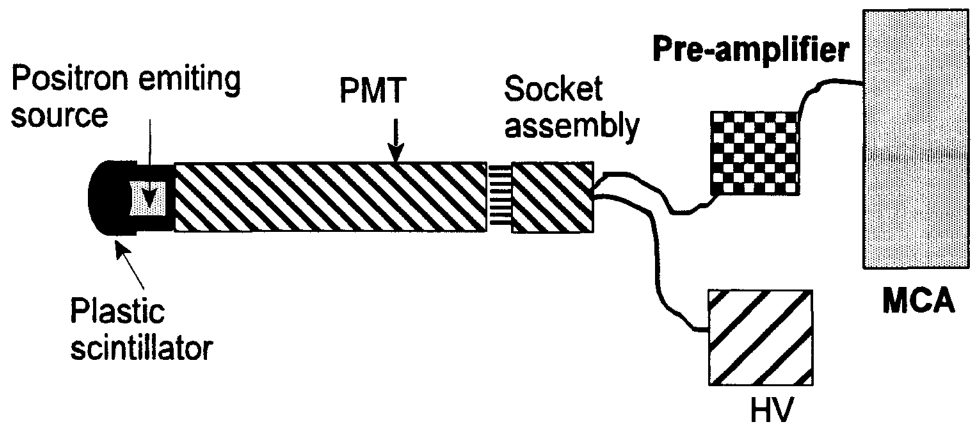

2. Advantages of the beta-gamma system

Beta-gamma coincidence transmission scanning has several advantages over the standard method of using orbiting rod sources. In beta-gamma coincidence the event rate is no longer limited by the count rate of the detectors nearest the source for the same reasons as the ^{137}Cs method. This allows the source strength to be increased therefore leading to more accurate transmission scans. Beta-gamma transmission scans are also estimated to be more than a factor of ten faster than orbiting rod source scans since they share the same advantage as the ^{137}Cs single method of being able to turn off the nearest detectors [25]. As such the event rate is determined by the sum of the single detector rates on the far side of the source. Using the beta-gamma technique reduces the need for more precise energy discrimination and longer pulse shaping time since almost all the near detector photons will have a known origin. The effects of random events will also decrease in beta-gamma scans thanks to the known locations of the annihilations and beta-gamma scans additionally allow post-injection scans without adding extra random events. In the beta-gamma method there is no longer a need to rescale the energy as required in the ^{137}Cs single method scan which involves complicated programming before or during reconstruction. Finally this technique allows for the use of multiple sources thus enabling the entire scan field to be covered as opposed to ^{137}Cs source method. This is possible since the LORs are formed by joining the present location of the source to the detector which records the gamma rays thus eliminating the problem of axial coverage.

3. Beta detection versus gamma detection

Beta detection and gamma detection are fundamentally different. In order to fully understand the differences between the two, a detailed description of both a gamma and a beta spectrum is necessary.

Gamma spectrum

As mentioned in Chapter 1, the result of a Compton scattering interaction is the creation of a recoil electron and a scattered gamma-ray photon. All scattering angles usually occur, therefore a continuum of energies can be given to the electron from zero up to the maximum predicted by the Compton equation (see Chapter1). The maximum energy that can be transferred to this electron represents the Compton edge and all the energies from zero to the maximum represent the Compton continuum as shown on the spectrum in Figure 25.

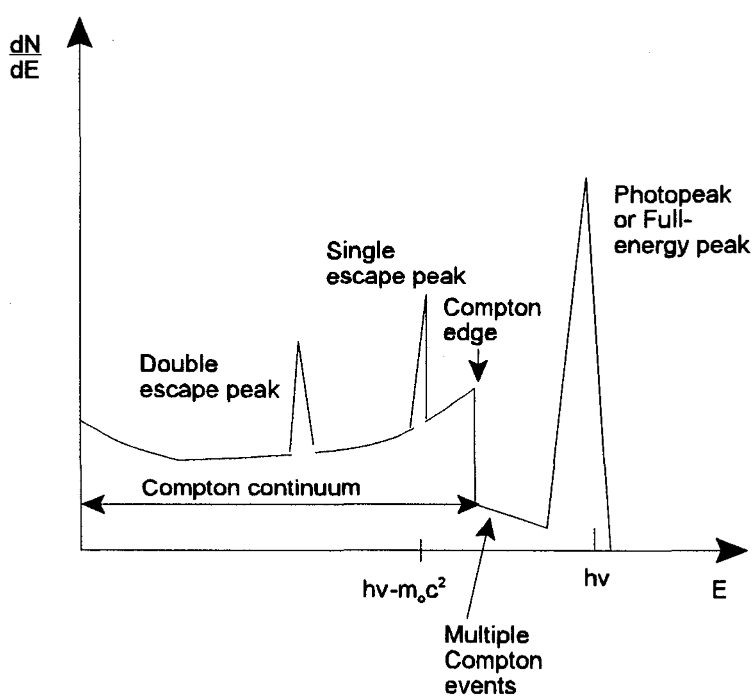

Figure 25 Gamma ray spectrum

The process of photoelectric absorption is also observed in the spectrum by giving rise to a photoelectric peak called a photopeak. Finally at high energies, the pair production process adds single and/or double escape peaks to the spectrum. The single peak corresponds to pair production interactions in which only one annihilation photon leaves the detector without further interaction whereas the double peak is due to pair production events in which both annihilation photons escape. It should be noted that for 511 keV events these peaks would not appear since the minimum energy required is $h\nu - m_o c^2$. In gamma ray detection the energy transmitted to the crystal from these interactions is used for detection. This energy is usually detected by placing an energy window around the photopeak. Thus the gamma detection system is very dependant on an accurate detection of the full photopeak .

Beta detection

Compared to gamma ray detection, the beta spectrum is fairly "simple". The continuous electron distribution from a beta emitter is shown in Figure 26.

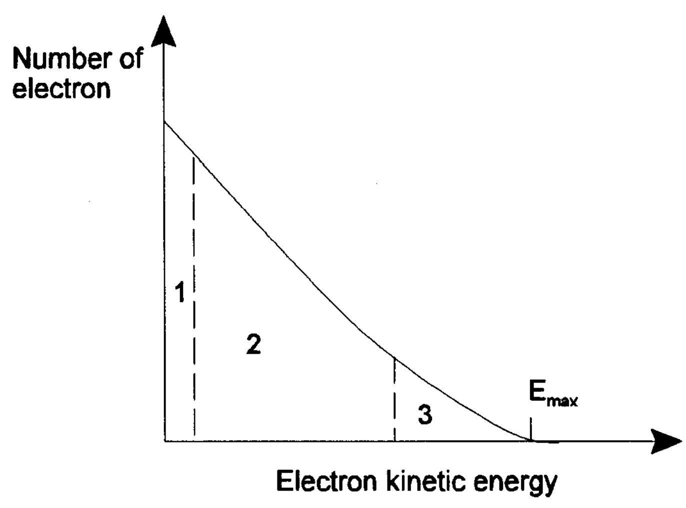

Figure 26 Beta decay spectrum

The beta particle that is ejected from a beta active nucleus may have any energy from zero up to a maximum value characteristic of the parent nucleus. The beta particle and the neutrino which is also ejected with each beta disintegration share the energy released by the nucleus but this energy can be distributed in any way between them. In beta decay detection the full spectrum does not need to be recorded. The beta particle will interact with the medium causing some energy loss as it travels and eventually it will lose all its energy and come to rest. Thus recording only the middle part of the spectrum (represented by part 2 in Figure 26) is sufficient for detection. Although the low energy beta particles that are present in part 1 will not be detected most of detected counts in this part of the graph represent noise and therefore should not be considered. The particles in the third part of the graph represent high energy beta particles that have already lost some energy through previous interactions and thus were detected already.

In the plastic cylinder used for our beta detection, the wall thickness does not need to correspond to the positron range as long as enough thickness is provided for the positron to interact. As a result of this, a thin wall of steel will surround the overall cylinder so that all the annihilations take place inside the known volume.

3. Overview of the PIN diode method used to detect beta-gamma coincidence

Early methods of beta-gamma coincidence transmission scanning conducted by our group made use of PIN photo-diodes to detect the positron emissions from a ^{18}F source [38]. The authors of this study suggested that an active source could be made by sandwiching a thin film (on which drops of ^{68}Ge had been painted) between pairs of PIN diode. Results demonstrated that PIN diodes can be used in beta-gamma coincidence with very good results. The timing resolution between the PIN diode detection and an LSO crystal connected to a PMT was as small as 5.9 ns. The goal of the present study is to demonstrate that beta-gamma detection using a plastic scintillator is at least comparable to the results obtained using the PIN diode method. Additionally, the use of a cylinder made of plastic scintillator should give better results with full coverage of the source as opposed to sandwiching it.

4. Methods used for our beta-gamma detection

In order to efficiently detect the beta decays attempts were made to entirely cover the 4π area around the source with scintillating material. Initially, multiple plastic scintillator fibers were placed around the source while later designs made use of a machined source holder in the shape of a cylinder made of plastic scintillator. Details of both designs will be given later in this chapter.

II. NUCLEAR INSTRUMENTATION MODULES USED

As indicated in Figure 24, positron detection required the used of several nuclear instrument modules (NIM). A brief description of each module and component used is given below.

1. Pre-amplifier

Pre-amplifiers are designed to provide gain close to the experimental detector before the signal-to-noise ratio is permanently degraded by cable capacitance and pickup. The pre-amplifier minimizes noise and pickup in the connecting lines and reduces measurement time in noise limited experiments.

2. Constant fraction discriminator

After the pulses have been magnified to a useful size by the pre-amplifier they are ready to be presented to a discriminator. In our system the discriminator uses a constant fraction of the signal amplitude as a threshold and thus will not pass pulses below a certain height. The constant fraction discriminator analyzes the peak amplitude of the energy pulses from the pre-amplifier with energy levels determined by front panel controls. For every pulse fed into it, the discriminator gives a fixed height output pulse if, and only if, the pulse height is above the discriminator level. A fixed output independent of rise times or amplitudes is achieved by deriving a zero crossover obtained by summing the original pulse and a delayed, inverted and amplified version of the original pulse so that all signals will cross through zero at the same time.

3. Analog to digital converter

An analog to digital converter (ADC) generates a digital word proportional to the amplitude of the input signal. The ADC is not used directly in the beta-gamma detection setup but is part of the ANIPET hardware that was used to test our beta-gamma attenuation correction system. The principal characteristics of the ANIPET will be briefly explained later. The ADC converts all the coincident signals received from the two position sensitive PMTs used in the ANIPET into digital words which are saved into a list-file corresponding to the detector position and the time of the coincidence event. These signals include position information (X and Y coordinates) and energy information for each coincidence. These same values will be used in our program for attenuation correction.

4. Delay box

One of the simplest modules, the delay box simply delays the given linear or logic signal by a time determined by front panel controls. This module is very useful in timing spectrum measurements. It allows us to calibrate the multichannel analyzer channels so that a time channel conversion is obtained.

5. Time to amplitude converter

The time to amplitude converter (TAC) is an essential component when preforming timing applications. The TAC produces an output pulse with an amplitude directly proportional to the time difference between two specific events (a start and a stop input pulse pair). The output of a TAC may be treated in the same manner as energy pulses to derive information concerning the time distribution, resolution or correlation of events.

6. Pulse height analysis

The pulses exiting the pre-amplifier are proportional to the energy that the positrons deposit in the crystal. Accordingly, if these pulses are sorted in terms of their heights it will be equivalent to sorting the positrons according to their energy. This technique is called pulse height analysis and the electronic circuit that is used is referred to as a pulse height analyzer (PHA).

Single-channel analyzer

A single-channel PHA or single channel analyzer (SCA) examines only one range of gamma energies (called channels) at a time. This apparatus is adjusted using two important parameter controls: the threshold level and the channel width. The SCA measures the events that exceed the desirable threshold level and a standardized output pulse is generated. Discrimination of the pulses occurs below this threshold amplitude as well as above an upper threshold level determined by the channel width. As such the SCA only measures events occurring in a selectable energy window.

Multi-channel analyzer

A multi-channel analyzer (MCA) is simply an extension of a single-channel analyzer. Unlike an SCA, a multi-channel analyzer is capable of sorting out and displaying events in a large number of channels simultaneously. Typically, a cathode ray tube is used to display the full energy spectrum live. The MCA builds up a histogram of pulse heights by adding 1 to each bin each time a pulse of that amplitude arrives. It can thus produce either an energy spectrum or, if using a TAC, a timing spectrum. The spectrum can then be read out into a computer for further analysis.

III. ELECTRONIC DESIGN FOR POSITRON DETECTION AND COINCIDENCE

Implementation of the beta-gamma coincidence setup involved a considerable amount of electronics work in order to run the PMTs and to determine the positions of the sources used.

1. Pre-amplifier design

The two pre-amplifiers used during the project are shown in Schematics 1 and 2. The first one was used in conjunction with the R647 PMT in all the preliminary efficiency tests while the second one, which is faster and smaller, was used for all the final work done with the R1635 PMT. The specifications of these PMTs are given in Table 3.

Hamamatsu PMT R 647	**Hamamatsu PMT R 1635**
Size: 13 mm (diameter) × 71 mm (length)	Size: 10 mm (diameter) × 45 mm (length)
Gain: 1.1×10^6	Gain: 1.1×10^6
Active diameter: 10 mm	Active diameter: 8 mm
Peak Wavelength: 420 nm (range 300 - 650 nm)	Peak Wavelength: 420 nm (range 300 - 650 nm)
Negative high voltage: 1000 V	Negative high voltage: 1250 V
Rise time: 2.5 ns	Rise time: 0.8 ns

Table 3 Characteristics of PMT used for the study

Schematic 1 Pre-amplifier used for PMT R 647

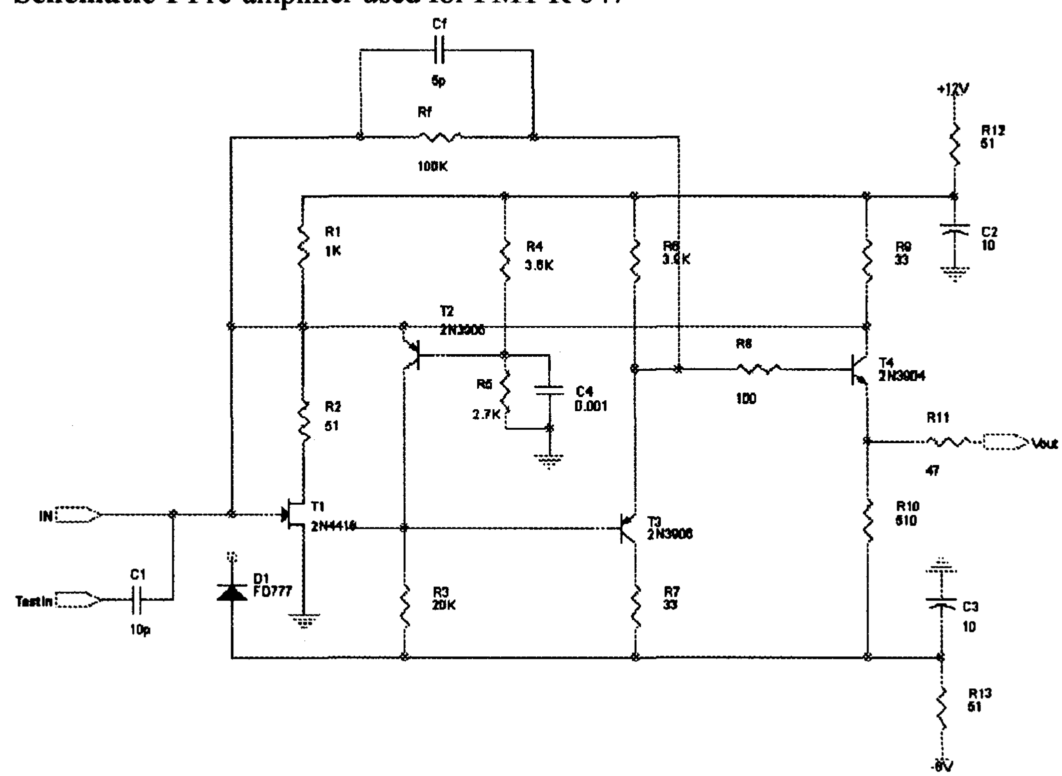

Schematic 2 Fast amplifier used for PMT R1635

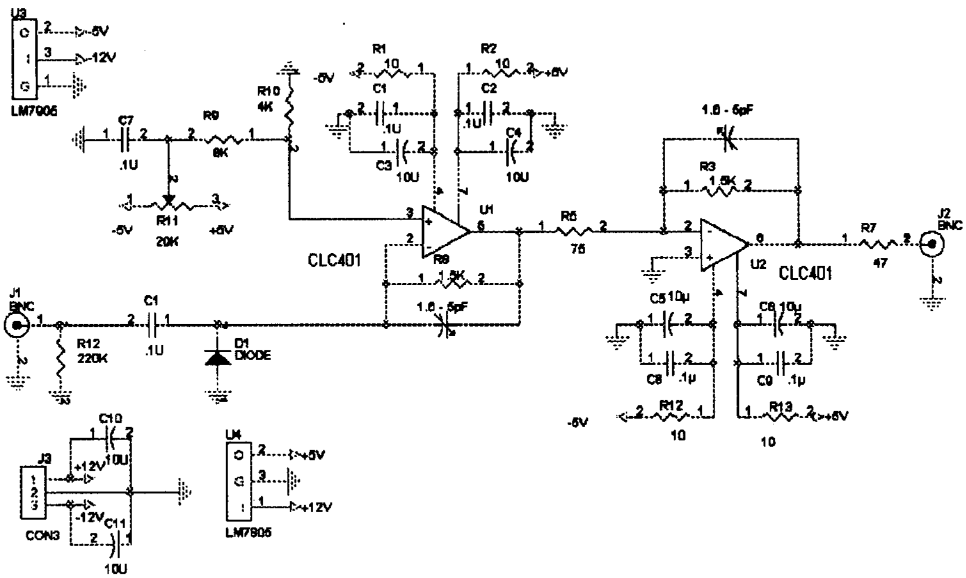

Pre-amplifier design is largely dependent on the type of signal being processed. One problem encountered during setup of the system was the configuration of the pre-amplifier used. Prior to use in this setup this pre-amplifier was fed by a positive high voltage PMT whereas the PMT used in our project was negative high voltage. The schematics for the socket assemblies of typical negative and positive high voltage PMTs are shown in the Figures 27 and 28. In the negative polarity PMT the anode is grounded and the cathode is at a high negative potential whereas in the positive polarity PMT the cathode is grounded and the anode is at a high positive potential. First attempts at using the pre-amplifier resulted in an interesting problem. The pre-amplifier worked for a very short period of time after which the signal would decrease to 1/10th of its initial value. In the positive polarity setup the anode is always positive thus allowing the electrons to easily go from one dynode to another. In the negative polarity setup, however, the cathode directly connected to the negative high voltage emits electrons toward the anode. Between each dynode a potential difference has to be maintained in order to direct the electrons toward the anode. Unfortunately the anode of our PMT socket was not grounded (see Figure 27) so although initially the potential difference between the electrons at the anode and the last dynode would give a normal output, after a few minutes the anode, not capable of discharging itself, would reach the same potential as the last dynode and the circuit would be frozen. In order to resolve this problem the anode was connected to ground through a high resistance thus enabling it to discharge itself.

Figure 27 Negative PMT socket

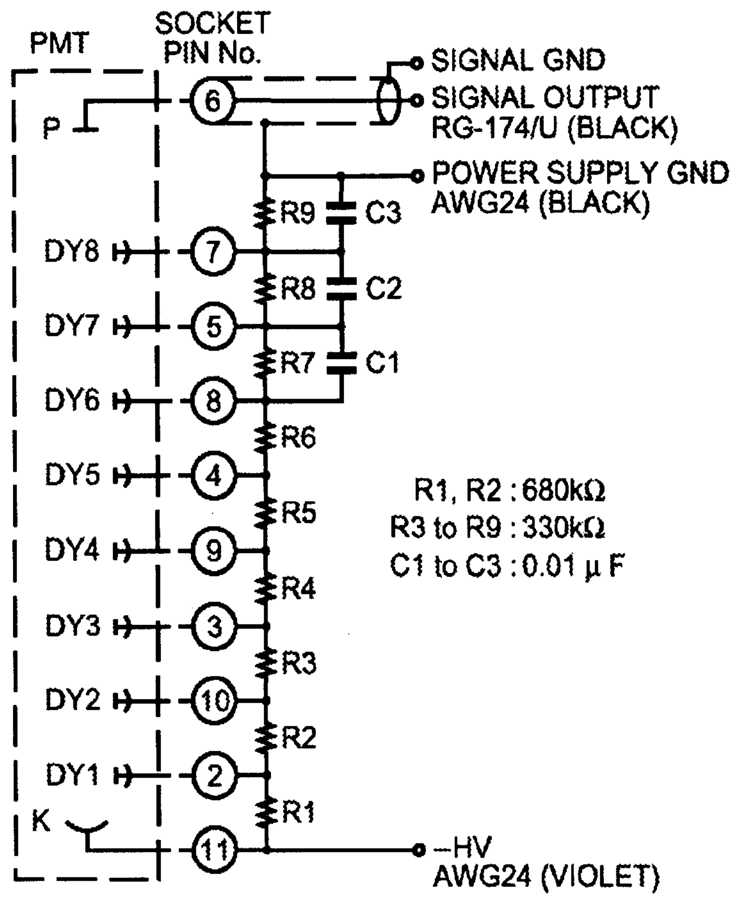

Figure 28 Positive PMT socket

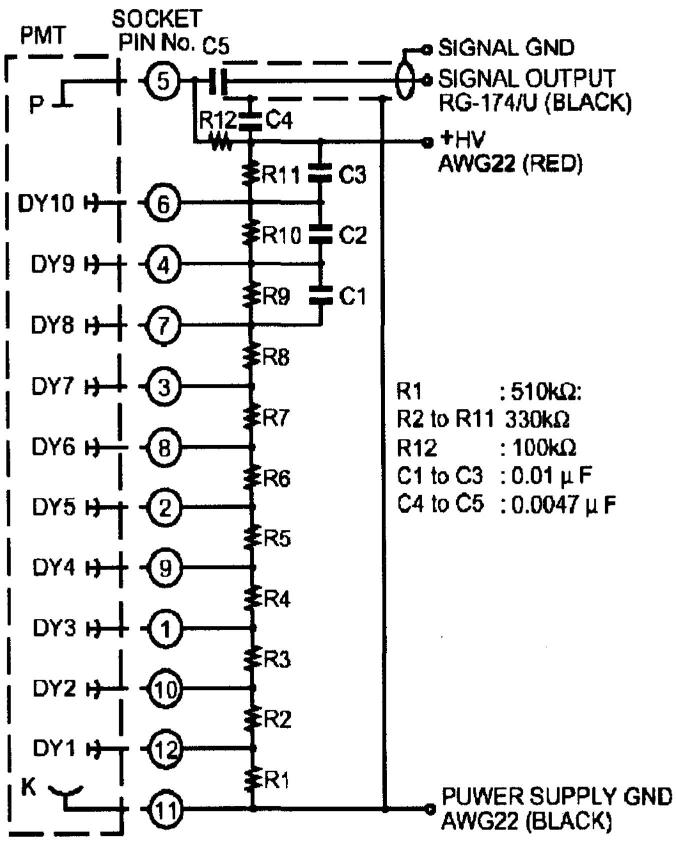

2. Positron position in the transmission box

In order to accomplish precise attenuation correction, each positron emitting source position must be accurately known. The positron position circuit operates as follows. Each source produces a signal all of which are treated in the same way through the PMT. The signals then proceed through the pre-amplifier and the constant fraction discriminator and are finally sent to an OR (SN74LS32N) circuit. This device contains four independent 2-input OR gates. The OR gate receives signals from each PMT and gives an output only if one signal occurs at a time. This avoids the inconvenience of attempting to process two signals at the same time which could lead to problems with our program in distinguishing them. Distinguishing which signal the OR gate has allowed to pass is accomplished by applying a different resistance to each signal. The resulting voltage from the signal is then analyzed thus identifying the PMT and the corresponding source position is fed into the computer for attenuation correction analysis. Further on in the study an alternative, more complex method of resolving the source position was used. This method, the schematics and the reasons for changing to it will be described later.

3. Conception of a coincidence module

The design and the construction of the coincidence module for the particular purpose of detecting coincident beta and gamma rays is illustrated in the schematics on the following pages.

<u>Schematic 3 and 4</u>

This part of the coincidence module takes the signals from the four positron sources coming from the quad CFD Ortec 934 (NIM output) and converts them to a TTL signal (logic signal). It then sends them to the actual coincidence system shown in Schematic 5.

<u>Schematic 5 and 6</u>

In order to make this coincidence module work, several calibrations and measurements were necessary. In the last schematic, which gives an overview of the entire coincidence module, the inputs 5, 6, 7 and 8 do not arrive at the same time as the inputs from the CFD of the ANIPET (inputs 9 and 10). Thus if no further modifications are performed, the coincidence will simply not work. In order to avoid this problem accurate measures of the time between the source detection on the cathode of the ANIPET's PMT and the input of the coincidence module are needed.

<u>Measurement of the time for a signal to reach the coincidence module</u>

Measurement of the time delay between the beta gamma detector and the coincidence module was accomplished by using a pulser directly fed into the pre-amplifier given in Schematic 2. This setup is illustrated in Figure 29. Triggering on the pulser signal, the oscilloscope readout of the time difference between the pulser and the pre-amplifier output of the whole beta gamma system indicated a 15 ns difference. The time becomes about 80 ns when the signal from the pre-amplifier is passed through the CFD. If the pulse comes from a positron source inside the plastic scintillator placed on the R1635 PMT instead of the pulser, extra time due to the PMT's electron transit time has to be taken into account. The electron transit time corresponds to the time interval between the arrival of the light pulse on the photocathode and the instant when the anode output pulse reaches its peak amplitude. This time is 9 ns for the PMT R1635.

Measurement of the time between the source detection and the output of the CDF for the ANIPET system cannot be performed in the same manner since the use of a pulser is not possible. In order to measure this time the beta gamma pre-amplifier output was used as a trigger and the difference between this signal and the output of the ANIPET's timing amplifier module was measured. The positron source is placed between the two detectors so that both of them will detect a signal coming from the same source. The time difference measured was 80 ns with no differences found between the two beta gamma pre-amplifiers. In order to evaluate the time for the ANIPET to detect the source, the time between the beta gamma's pre-amplifier and the source has to be added to the time difference between the beta gamma pre-amplifier and the ANIPET's timing amplifier module.

This gives us a total time of 80 (beta gamma pre-amplifier to ANIPET's timing amplifier) + 15 (pulser to pre-amplifier) + 9 (electron transit time) + 50 (CFD) = 154 ns whereas the total time for the signal to reach the coincidence module through the beta gamma system only takes about 89 ns (80 + 9).

Thus the beta gamma's signal has to be delayed before it reaches the coincidence module. In order to accomplish this a stretcher was used.

Schematic 3 Input from CFD,NIM to TTL

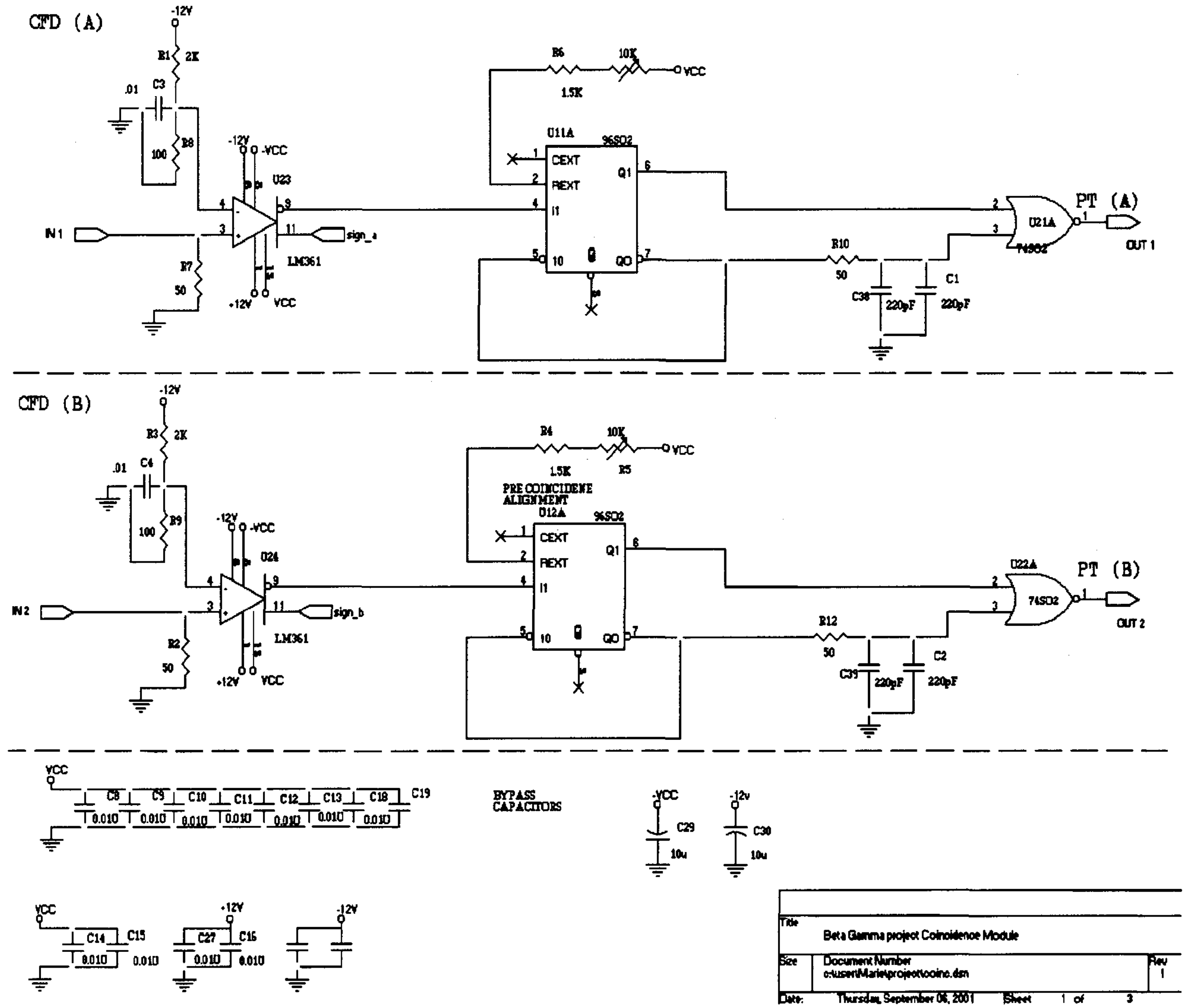

Schematic 4 Input from CFD, NIM to TTL

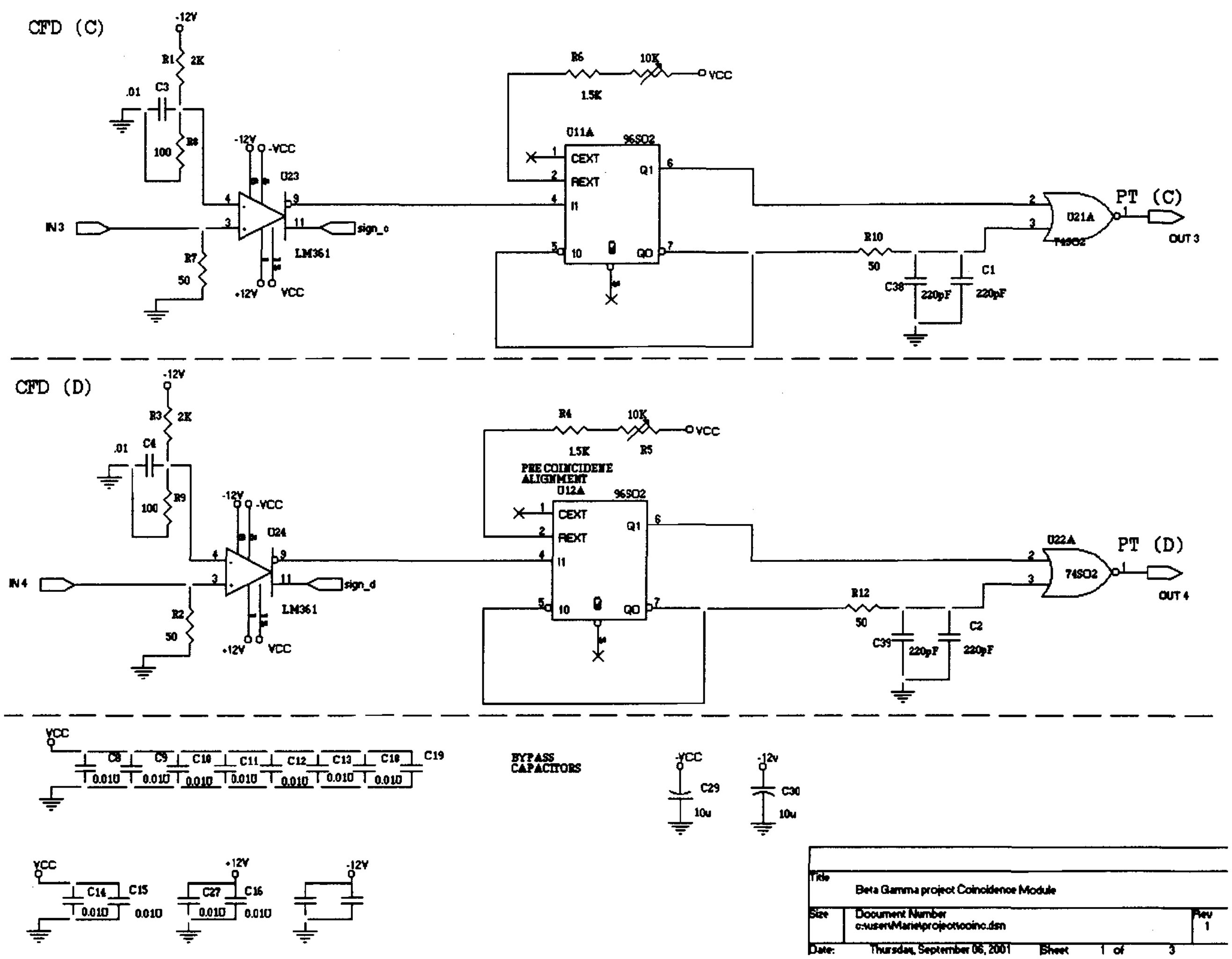

Schematic 5 Strobe to ADC

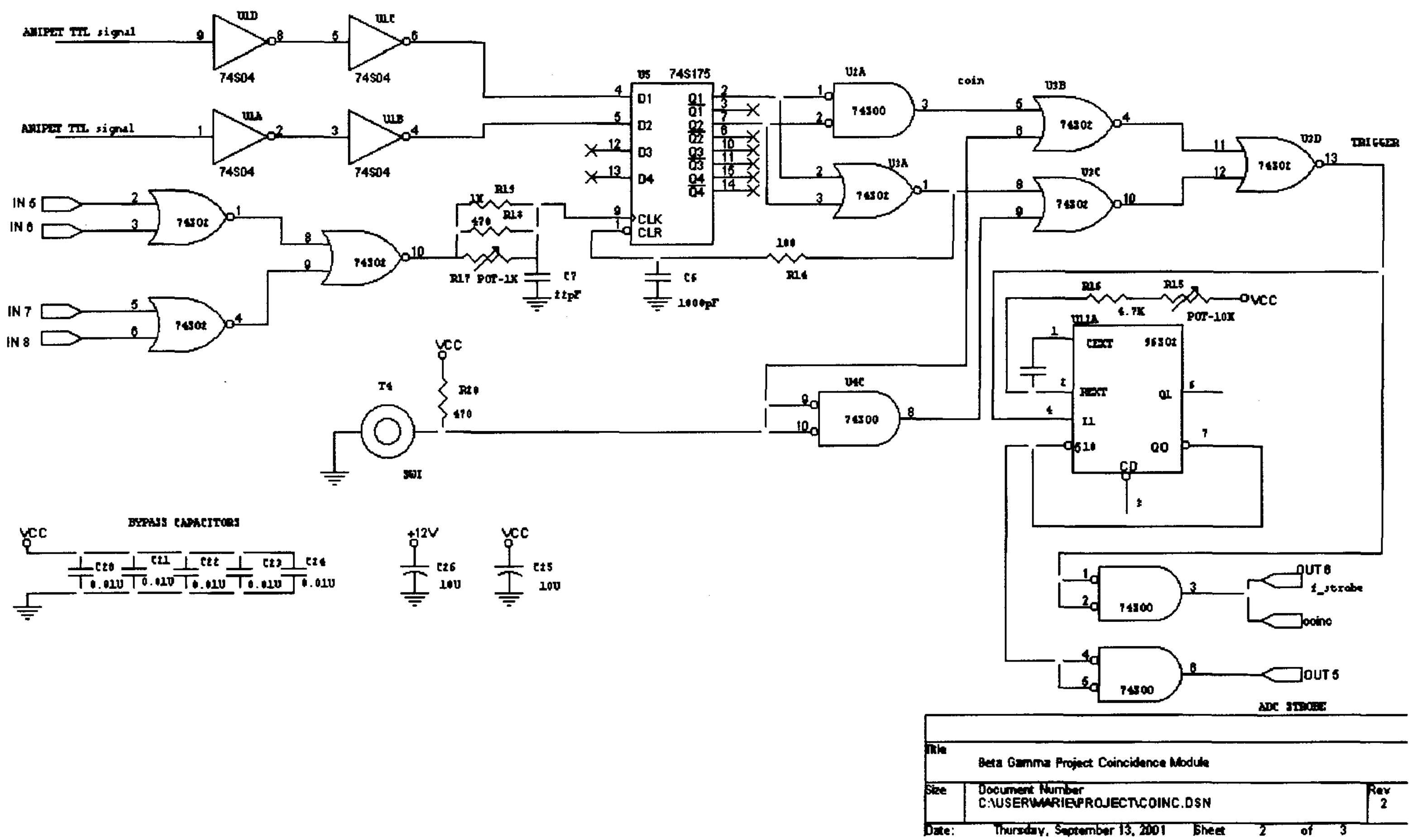

Schematics 6 Coincidence module

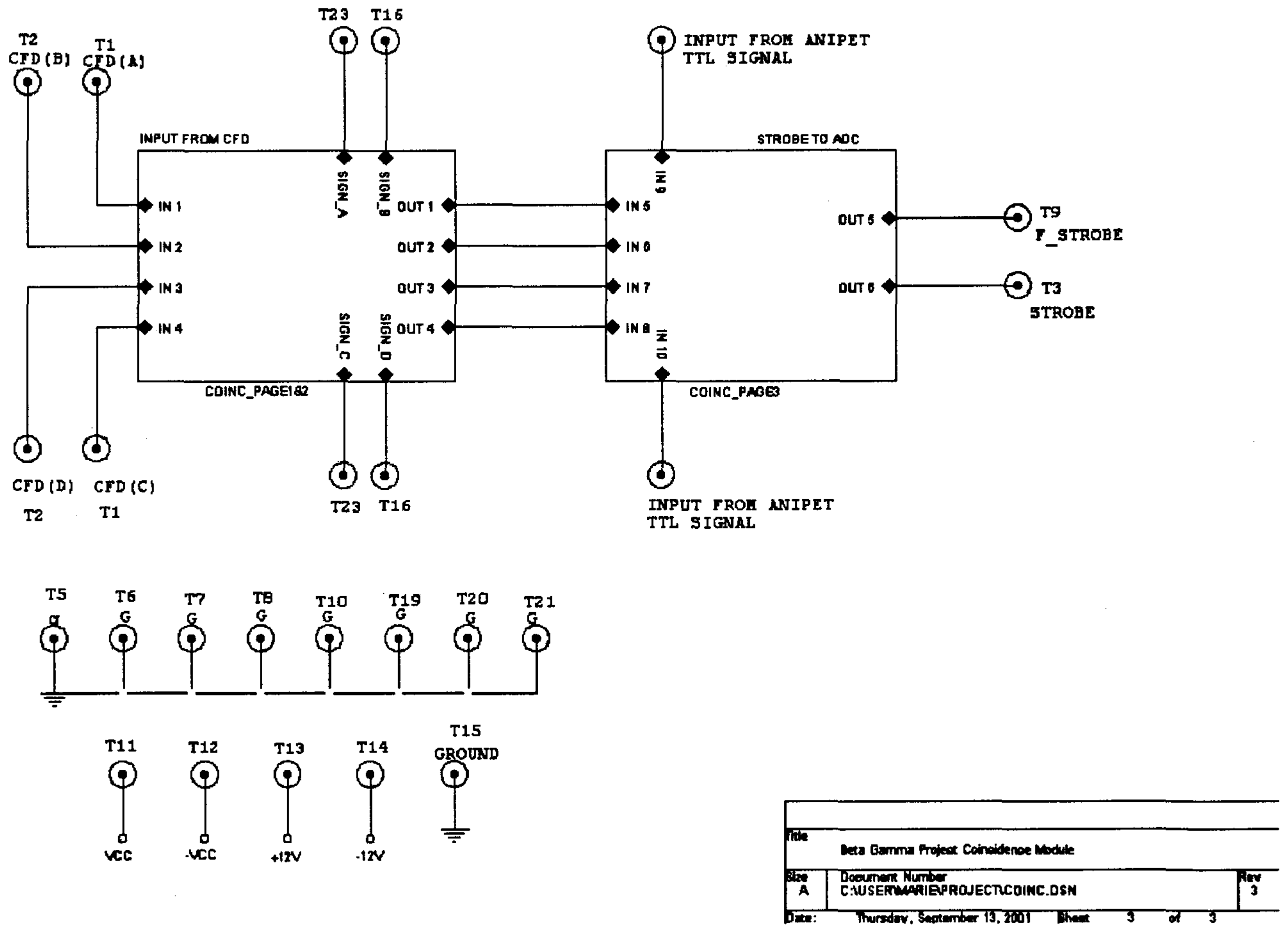

Figure 29 Measure of time interval between different part of the system

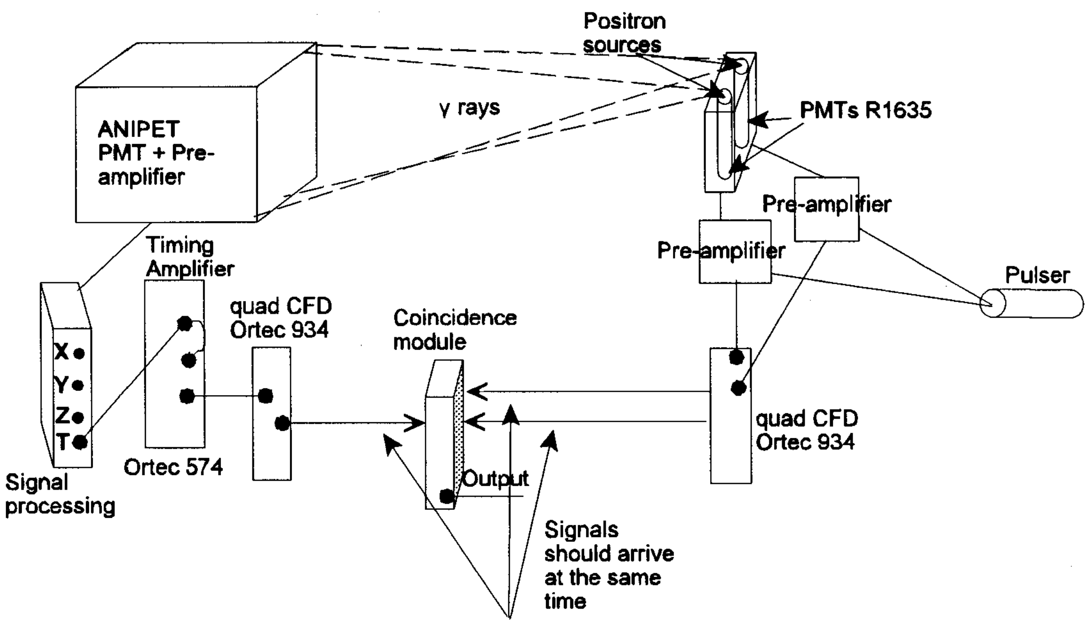

Stretcher

By adjusting the resistance and the capacitor to the proper value the signal from the pulser can be stretched as shown in Figure 30 below. In this manner, the signal from the beta gamma detector was stretched by approximately 65 ns.

Figure 30 Stretcher

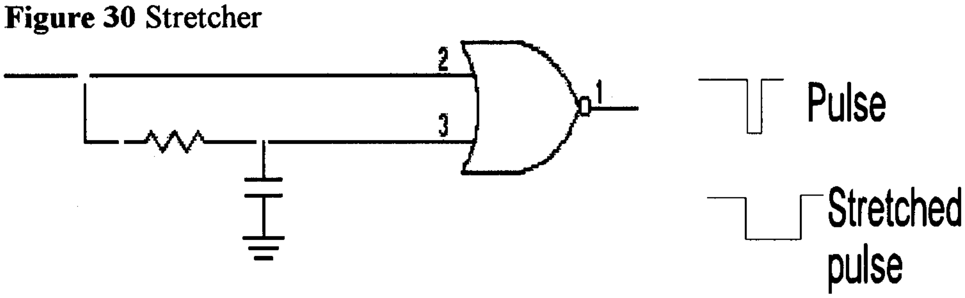

VI. POSITRON DETECTION METHODS / MACHINING

Constructing the new attenuation correction system involved several different aspects of mechanical and technical design. Described below are the different parts of our setup during its evolution and the special techniques involved in creating them.

1. Positron gel fabrication

The beta-gamma detection system required a solid positron source. Unfortunately the most commonly available positron emitting compounds are liquid and using an aluminum or steel positron sealed source in this case would not be appropriate. In order to overcome this problem we employed a method first devised by Murthy *et al.* [39] to fabricate very small wall-less positron emitting hot spots. The hot spots are made by adding ^{18}F-FDG or ^{11}C to a solution of Agarose (25 mg per milliliter of water). Agarose is a complex carbohydrate extracted from seaweed widely used by molecular biologist in gel-electrophoresis. Purified Agarose is sold in powdered form. At room temperature, it is insoluble in water but dissolves in boiling water. Upon cooling, the solution polymerizes and forms a gel similar to a gelatin. Typically, a 2 mm diameter hot-spot fabricated as mentioned above takes approximately two minutes to gel.

2. Scintillating plastic fiber network around the source

The positron gel source was initially surrounded by scintillating plastic fibers as shown in Figures 32 and 33. Through the use of a perforated holder, the fibers were placed in order to cover approximately 50% of the surrounding volume. Knowing that the approximate range of a positron is 2 mm, the fiber had to touch the plastic gel cylinder and the diameter of the gel itself could not be more than 2 mm. The fibers were then coupled to the PMTs so that the light could be detected and fed into the counting circuit. The final results were displayed on a multi-channel analyzer. A fibre optic light guide polishing tool was designed and machined to improve the coupling between the fibers and the PMT. As shown in Figure 31, the polishing tool was constructed from plexiglass to allow us to polish long or short fibers depending on the top layer used. Although the results obtained using this setup were very encouraging a more efficient setup was designed later in the project.

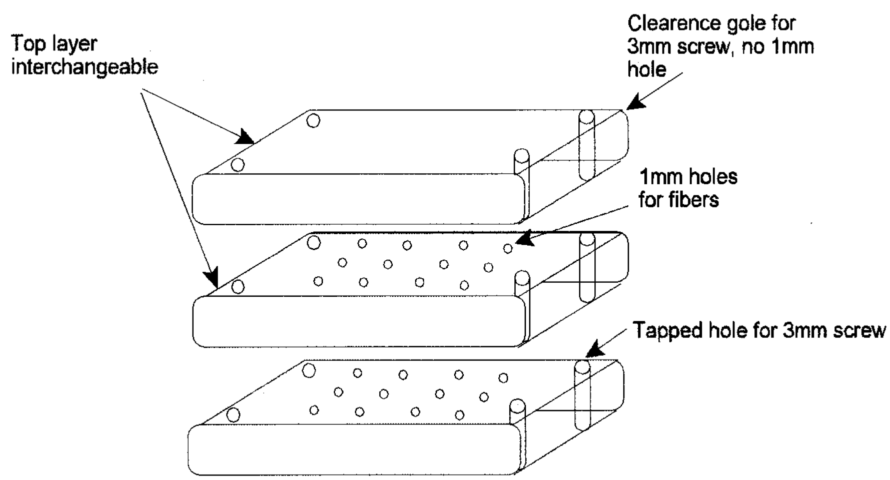

Figure 31 Polishing tool

Figure 32 Scintillating fibre arrangement

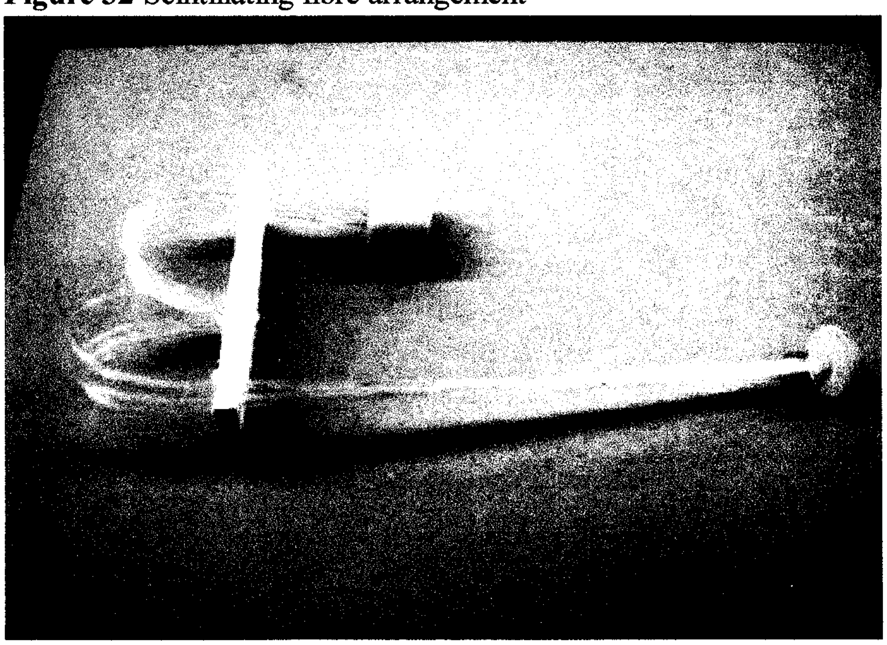

Figure 33 Scintillating fibre arrangement

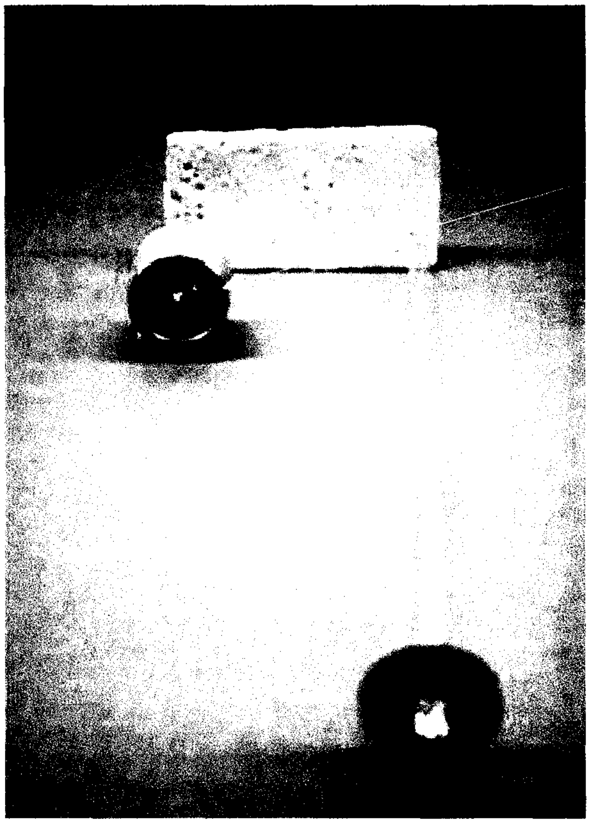

3. Design of a hollow cylinder made of scintillating plastic material

In order to increase the efficiency of the positron detection system attempts were made to increase the surface coverage around the source. The most successful of these attempts involved the design and fabrication of a hollow cylinder made of scintillating plastic material as shown in Figure 34. The cylinder walls were designed to have a 2 mm minimum thickness thus covering the positron range from the annihilation point anywhere in the gel while the hole had a 1 mm maximum diameter so that the radioisotope used, mainly ^{11}C with a range of 1.7 mm in water, would not annihilate inside the gel but inside the cylinder walls. Although thicker walls could have been used, this would have increased the contamination due to gamma ray interactions with the plastic scintillator and the cylinder had to be made as small as possible in order to behave like a point source.

Figure 34 Hollow cylinder made of plastic scintillator

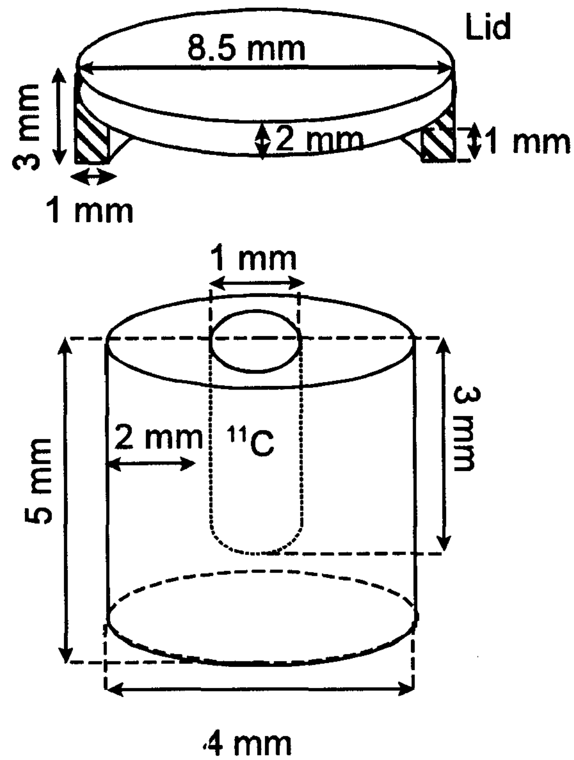

4. Design of the transmission box

Since the final goal of this project was to obtain attenuation correction images, a transmission box was designed so that the overall system could be implemented on the ANIPET. Optimally a transmission box should be small, light tight and the PMTs should be easily removable so that the hollow cylinder containing the short half life source can be easily changed. These requirements were achieved by machining the transmission box from a single block of black UHMW plastic. The design and dimensions of this box are shown in Figure 35. Four small PMTs (Hamamatsu R1635, 10 mm diameter) can fit inside the holes made inside the plastic block with the length of each hole drilled so as to cover the crystal area of the ANIPET detector. Each source acts as a transmission source and the whole setup is made to rotate around the animal. The top of the transmission box has been designed so that the

PMTs can easily be removed thanks to the use of black chemistry flask stoppers used as individual lids for each PMT.

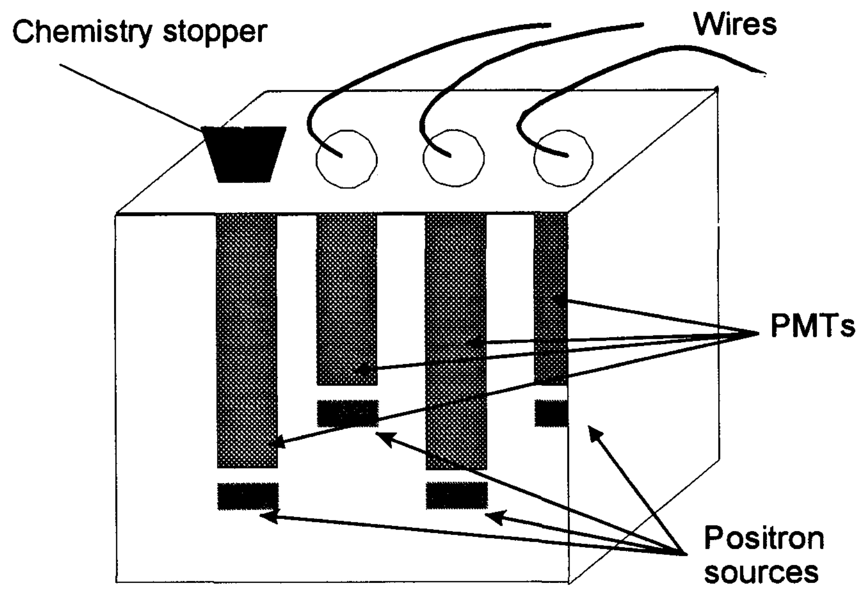

Figure 35 Transmission box

5. Implementation on the ANIPET

In order to produce accurate attenuation values the transmission system must rotate around the subject. The animal PET scanner (ANIPET) design, geometry, and components have been described by Thompson [27]. Briefly, the system consists of two planar detectors operated in coincidence. Each ANIPET detector module consists of four 36×36×20 mm pixilated BGO crystal arrays coupled to a 72 mm square position-sensitive photomultiplier tube (PS-PMT Hamamatsu R3941-5). These detectors are mounted on a horizontal metal shaft which is rotated by a stepping motor. The subject bed is mounted on a translation stage which is also driven by a stepping motor. The movement and position of these motors are controlled and monitored by the ANIPET acquisition software. The transmission setup is attached to the ANIPET as shown in Figure 36. A rectangular piece of metal has been added to one of the ANIPET detectors with four holes in order to fix the transmission box onto the

ANIPET detector. This transmission box can be easily removed for emission scans.

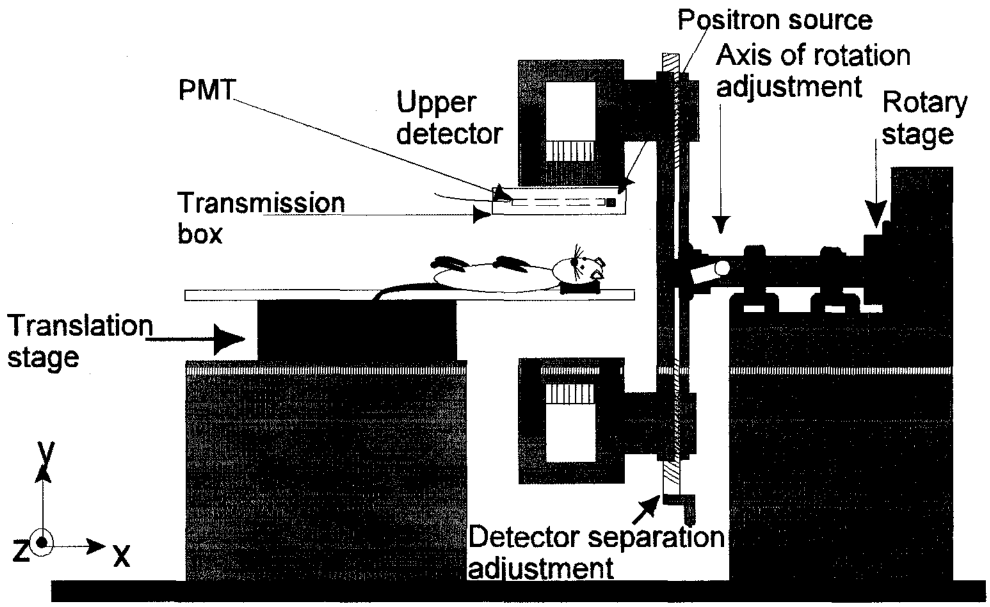

*Detectors contain collimators / PMT / crystals

Figure 36 Transmission box mounted on ANIPET scanner [2]

CHAPTER 4

TESTS PERFORMED ON THE BETA-GAMMA SYSTEM

I. TESTS PERFORMED ON PARTS OF THE SYSTEM

1. Timing spectrum calibration to measure resolution time

The beta-gamma performance was partly evaluated by setting up a timing spectrum between our setup and one of the ANIPET detectors. The most important characteristic of the timing spectrum is the resolution time. The resolution time is determined by measuring the full width half maximum (FWHM) of the obtained time spectrum curve. The full width half maximum is commonly used to describe a measurement of the width of an object in a picture, when that object does not have sharp edges. The FWHM is given graphically as shown in Figure 37.

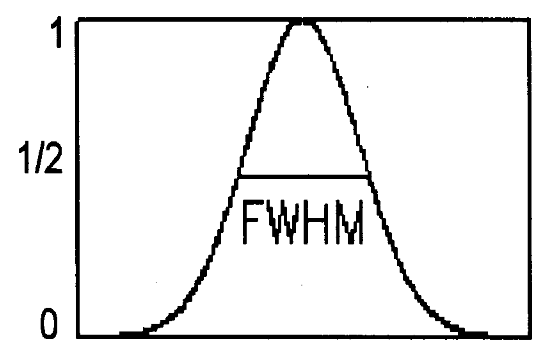

Figure 37 FWHM of a curve

In order to be able to measure the FWHM, or resolution time, of a spectrum obtained on an MCA, a channel to time conversion has to be calculated. This conversion was obtained by setting up the circuit shown in Figure 38. The same signal is fed into both inputs of the TAC with one of them delayed by a known amount. The acquisition is then performed with and without a delay. The time difference between the two graphs obtained gives the number of channels read from the MCA which corresponds to the delay between the two signals.

Figure 38 MCA channel to time converter circuit

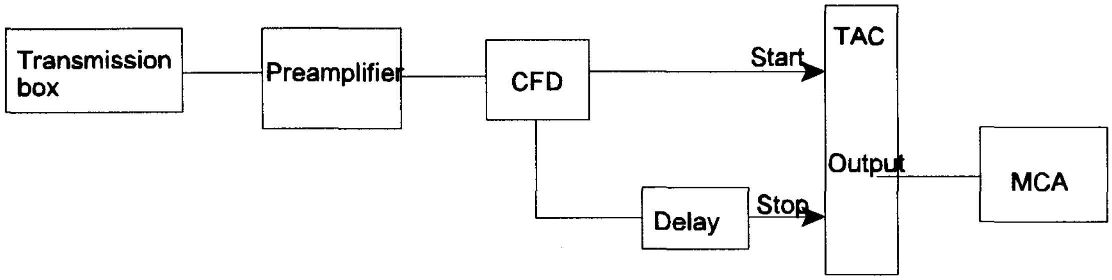

2. Calibration of different parameters

<u>Coincidence delay</u>

In order to properly perform a coincidence technique the resolution time of the coincidence module must be set to the proper value. A delay curve is obtained in which coincidences are measured as a function of relative delay between the two detectors. Another method would be to simply use a TAC to measure the time difference between the two.

<u>High voltage calibration</u>

The coupling between the plastic scintillator and the PMTs changes every time the ^{11}C source is renewed inside the scintillator cylinder. Since different coupling implies slight differences in the pre-amplifier pulses, each source has to be calibrated with every source change by adjusting the high voltage so as to avoid saturation problems. Calibration was performed by optimizing the appearance of the pulses on an oscilloscope and the beta spectrum on an multichannel analyser.

3. Possible noise measurements from gamma ray interactions

The beta detection system implemented here has the potential of being sensitive to noise resulting from gamma ray interactions. There are two such noise contributions which may constitute major sources of noise to the system. The first one comes from possible interactions of the annihilations photons directly with the plastic scintillator. Gamma ray interactions with fibre optics or clear optical guide have been studied in the past and have been found to be significant [40]. The second contribution comes from possible Cerenkov radiation contamination. Cerenkov radiation is produced when a charged particle passes through a medium of refractive index n with a velocity greater than that of light in this specific medium. The physical characteristics of Cerenkov radiation have been extensively documented [41, 42] and will only be briefly reviewed here The angle θ at which the Cerenkov radiation is emitted relative to the particle's direction is given by:

$\theta = \arccos(1 / n\beta)$ with $\beta = v / c$

In order to check the possible interactions of gamma rays with the plastic cylinder, we measured the spectrum of a 30 mCi source of ^{137}Cs placed close to the plastic cylinder.

II. TESTS PERFORMED ON OUR SYSTEM

1. Detection efficiency

In order to determine the detection efficiency the activity of a ^{11}C sample was accurately measured using a well-counter with a known efficiency and the results were compared to those obtained by our positron detection system. For this experiment we used the PMT R1647, with specifications given in Table 3 (see Chapter 3). This PMT was connected to a pre-amplifier and a multichannel analyser (MCA) which provided the number of counts per bin as an energy spectrum.

2. Attenuation measurement

Preliminary testing of the beta-gamma coincidence method was performed using the ANIPET. A block diagram of the configuration used in the attenuation test is shown in Figure 39. The positron detection is used to trigger a coincidence circuit in single mode with one of the ANIPET detectors. Early tests were made using different thicknesses of Lucite (linear attenuation: 0.092 cm^{-1} at 511 keV) placed between the positron detection system and the ANIPET detector and the attenuation was calculated by dividing the counts with the object in place by the counts acquired during a blank scan for each point in the sinogram. Two experiments were performed for this test as detailed in Table 4.

Figure 39 Block diagram of attenuation measurement

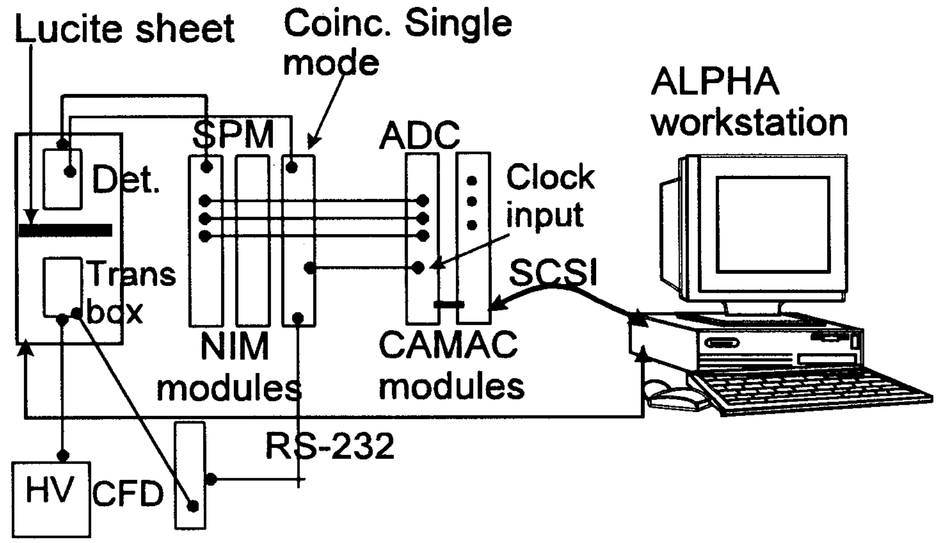

Table 4 Measure of attenuation efficiency

Experiment 1	Thickness	Acquisition time	number of buffer filled
Blank scan		5 min	280
Lucite 1	9.55 cm	5 min	200
Lucite 2	11.71 cm	12 min	400
Lucite 3	11.92 cm	7 min	170
Experiment 2			
Blank scan		16 min 30 s	6000
Lucite 1	9.55 cm	27 min 39 s	6000
Lucite 2	11.71 cm	12 min 26 s	3000
Lucite 3	11.92 cm	13 min 32 s	3000

3.Timing spectrum between the positron detector and the ANIPET detector

The timing performance of the positron detection was compared to a BGO crystal connected to a PMT (ANIPET detector) through the following experiment. A block diagram of the configuration used is shown in Figure 40. In this configuration, the signal coming from the beta detector is also sent to the quad CFD Ortec 934 and fed to the TAC as a START pulse. The ANIPET detector is connected through a signal processing module to a timing amplifier (Ortec 574) and then passed through a quad CFD Ortec 934. The signal is then delayed through the use of a NSEC (nanosecond) delay module from Canberra (model 2058). Finally the signal is connected to a time analyser (TAC) Canberra 1443A as a STOP pulse and the output is send to the MCA Tracer Northern TN_1705. Both the positron detection system and the ANIPET are fed with a high voltage power supply Canberra 3002D. The timing spectrum between the beta detector and the ANIPET was recorded with 0, 16, 32, 50, and 62 nanosecond delays using first a gamma source and then a 1 μCi sample of ^{11}C.

4. Measurement of beta energy spectrum

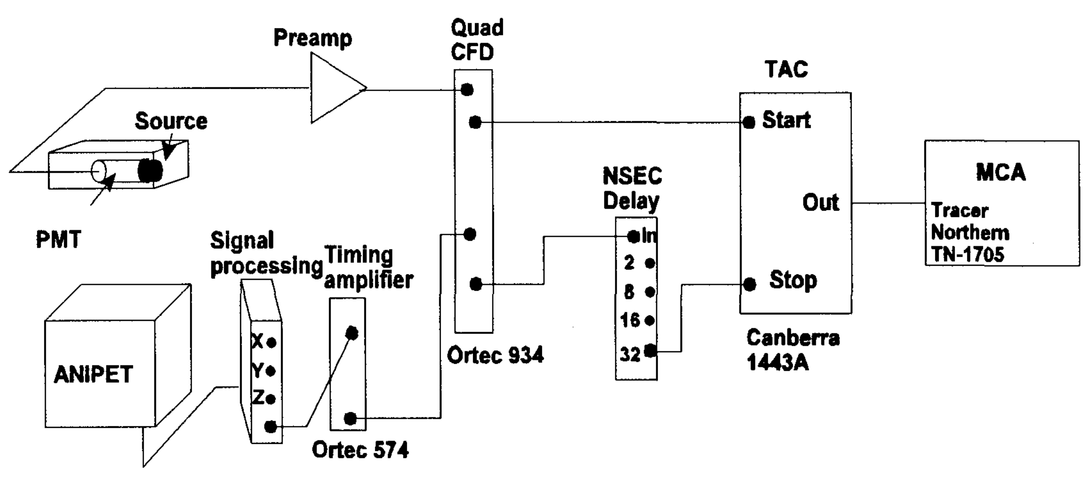

Figure 40 Block diagram of the components used for the timing spectrum

Measurement of the beta spectrum was performed by connecting the fast pre-amplifier used for the PMT R1635 directly to an MCA. Unfortunately our pre-amplifier output is negative while most MCA input accept only positive pulses. We thus converted the pre-amplifier output with an inverter and fed the inverted pulses to the MCA as shown in Figure 41.

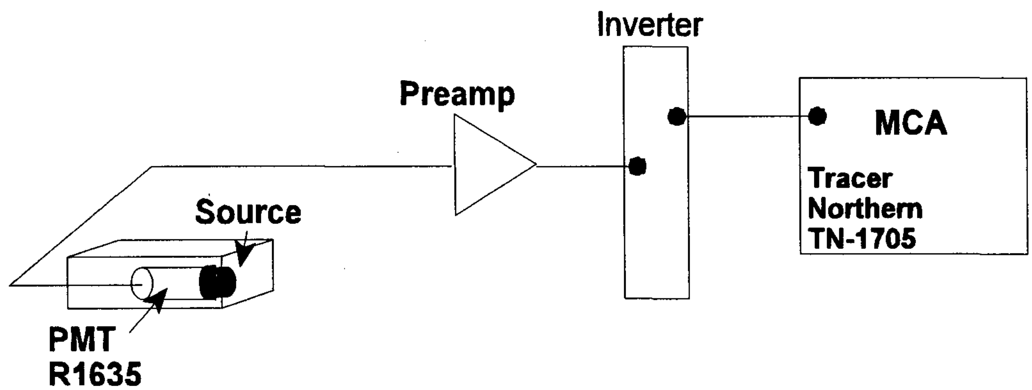

Figure 41 Block diagram of the beta spectrum measurement

5. Coincidence between beta detection system and the ANIPET

This test was performed using the setup shown in Figure 42. In this figure the source positions of the transmission box are numbered in order to explain the way each signal coming from each PMT is treated. The ANIPET program called Aurora_Spectrum_Display, or ASD, used to trouble-shoot and calibrate the detectors gives three images when a coincidence circuit is applied between the two detectors. The first two images are the view of the source distribution from each detector and the third one is the coincidence image reconstructed on a plane half way between both detectors. Instead of having the ADC strobe triggering the six channel 12-bit ADC to digitize the x, y, and energy signals of each detector for all coincidence events, the three unused channels from the detector were used to store the x and y source positions. These values were then saved into a list-file containing, for each coincidence event, the time of the event and the corresponding detector position. As a result, when the ANIPET program prints out the coincidence image between the positron set up and one of its detector, the image obtained gives an idea of the results we will obtain after reconstruction. This image provides an idea of the possible results of our coincidence circuit before the use of a particular reconstruction program. In order to obtain information from the third image we apply two operational amplifiers for each of the sources as shown in the Schematic 7. After going through the "x" operational amplifier circuit the signals from the sources in position 1 and 3 have negative voltage while the signals from positions 2 and 4 have positive voltage. The same relation applies to the "y" operational amplifier. By adjusting the resistences to the right value the circuit will give an approximate source position allowing the ANIPET program to reconstruct a coincidence image between one of its detectors and our system using the values stored in the list-mode.

Figure 42 Coincidence set up

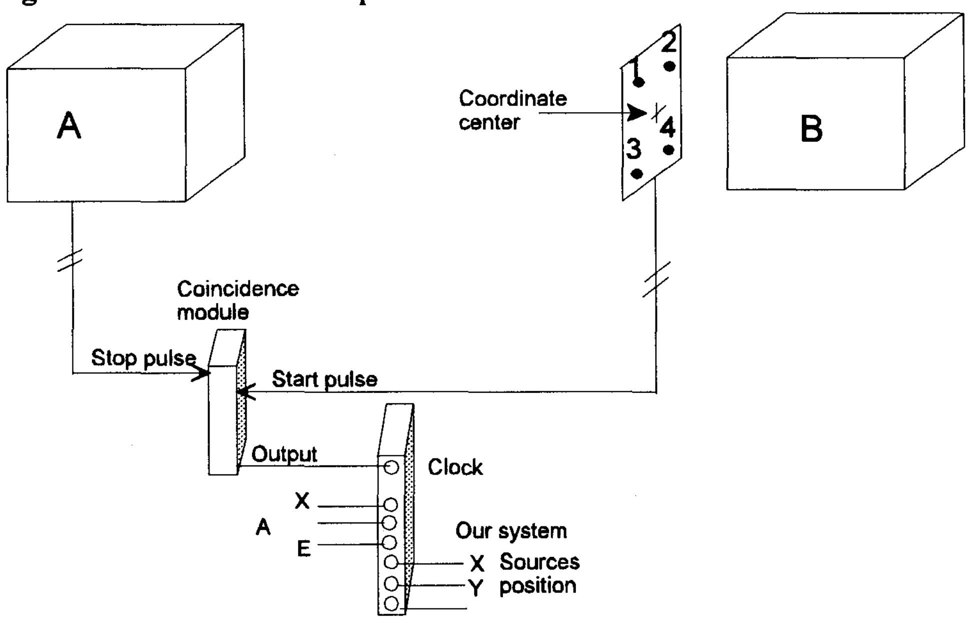

Schematic 7 Position source electronic circuit

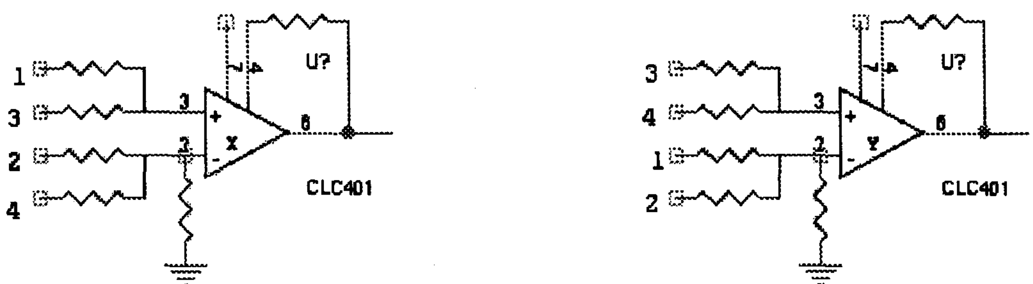

CHAPTER 5

RESULTS AND DISCUSSION

I. RESULTS OF THE TESTS PERFORMED ON PARTS OF THE SYSTEM

1. Possible noise measurements from gamma ray interactions

There was no meaningful noise found in the measurement of the spectrum of a 30 mCi source of ^{137}Cs placed close to the plastic cylinder. We can thus assume that there will be no significant noise contribution from gamma rays or Cerenkov radiation in any future experiments.

II. RESULTS OF THE TESTS PERFORMED ON OUR SYSTEM

1. Detection efficiency

Results from the detection efficiency test are displayed in Table 5. The average detection efficiency was found to be 75.24 % with a standard deviation of 2.76 %. One could compare this result to the single sensitivity of an LSO crystal coupled to a PMT as used by Jones *et al.* [30, 31] who reported a sensitivity of 425 kcps/mCi (1.14%). In order to make a fair comparison between our positron detection system and their design, details of both studies should be clarified. Jones' system only detected the photons coming from the useful beam of a PET scan which is about 1/5 of the full trans-axial capability. This was carried out through collimation of the beam by surrounding the source with a lead cone. As a result of this, Jones' detection efficiency is actually 1.14% of the useful beam whereas ours detects the full 4π emission. For direct comparison between the two systems our detection efficiency should be reevaluated to 15% (1/5 of 75%) which is still ten times better than Jones' method.

Table 5 Measures of detection efficiency

Efficiency Test	well counter t = 0	t =16 min	t =23 min
Activity	397080 counts/ 20s (well counter efficiency 2.5) 397080 × 2.5 / 20= 49635 Bq	28511.5 Bq	22370 Bq
Measured Activity		20665.5 ct/s	17439.5 ct/s
Efficiency		72.48 %	78 %

2. Attenuation measurements

Attenuation efficiency of our set up was tested with a program written by Dylan D. Togane using the data acquired during the two experiments described in Chapter 4.

The attenuation calculation programs use source code from the standard ANIPET software written by Dr. Thompson in order to calculate the weighting factors of the list mode data. This C and FORTAN program is called by a Matlab script (attenuation.m) that prompts the user to enter the file names and experimental variables, calculates, and displays the calculated attenuation value. The PLD.C file contains the program's entry point. Memory allocation and file IO are performed here. The input files are read a block at a time, and the FORTAN routines are called to apply the lookup tables to the input files, producing energy and weighting values for each detected count. The weighting values reflect the solid angle subtended by each detector element and the crystal element efficiency. The solid angle, efficiency, and energy tables are loaded by the LOAD_TABLES.FOR file. The APPLY_LOOKUP_TABLES.FOR file actually preforms the lookup operations. The PROCESS_LIST_DATA.FOR file is called by the C program and co-ordinates the table loading and application of the lookup tables.

Initial experiments produced results which differed by up to 29% from the theoretical attenuation value in water (0.092 cm^{-1}). These poor results were due of the large separation distance between the positron detector and the ANIPET detector as well as the relatively short acquisition time (about 16 minute acquisition for 1 μCi). In this study only 1% of the positrons detected were actually useful to the ANIPET detector. In order to account for these problems, the acquisition time was set longer and the separation between detectors was decreased. Using this configuration, acquired attenuation measurements had a 5.3% deviation from expected (tabulated) values. Although this is a large improvement over the initial measurements, we expect to have even less deviation in future attenuation results which will be acquired with still smaller detector separation thus inducing a higher count rate received by the ANIPET detector.

3. Timing resolution and timing spectrum using gamma source

The timing spectrum obtained using a gamma source is shown in Figure 43. This timing spectrum was recorded between the beta source system and the ANIPET detector with 0, 16, 32, 50 and 62 ns delays.

Figure 43 Timing spectrum using gamma source

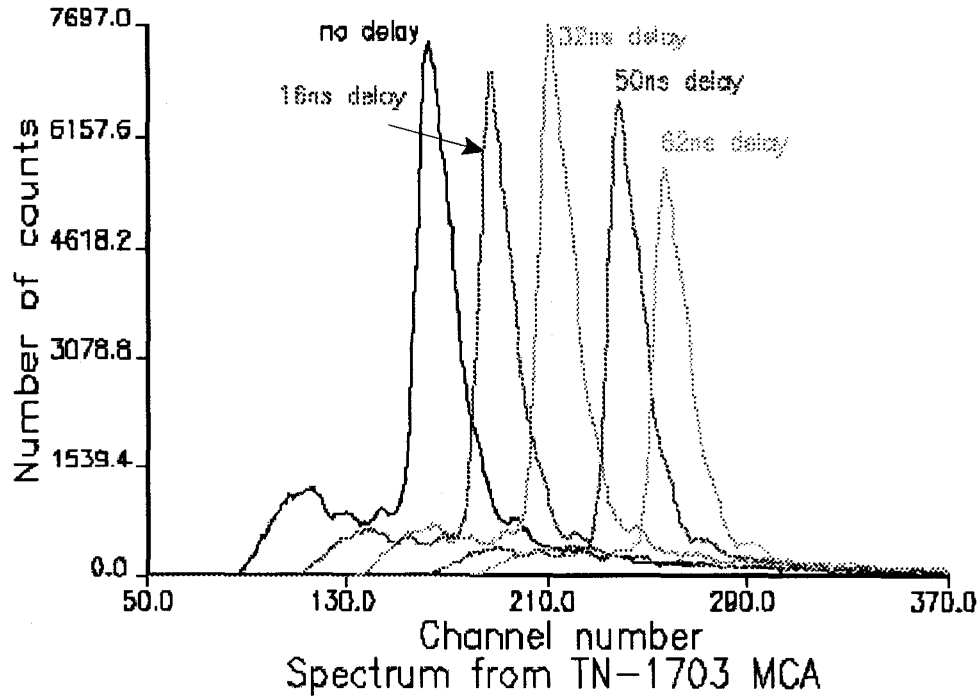

Each spectrum was acquired for 200 seconds using an aluminum sealed ^{68}Ge point source. A timing resolution of 11.5 ns was calculated using the list file of the graph.

4. Timing resolution and timing spectrum using beta source

The timing spectrum obtained using a beta source is shown in Figure 44. This timing spectrum was acquired with 0, 16, 32, 50 and 62 ns delays between the beta source pulse and the ANIPET detector. Each spectrum was acquired for 200 seconds using 1 μCi of ^{11}C. A timing resolution of 11 ns was calculated using the list file of the graph. There is a significant asymmetry in each peak recorded in the timing spectrum between the plastic scintillator used for beta detection and the ANIPET detector. This asymmetry can be observed by comparing the first half of the FWHM which represents the plastic scintillator resolution time (the rise time of the start pulse) with the second half of the FWHM which corresponds to the ANIPET resolution time (decay time of stop pulse). The first half of the FWHM of the peak ranges from 2.3 to 5 ns whereas the second half ranges from 6 to 9.9 ns. This huge asymmetry demonstrates how much faster a plastic scintillator detector (2.4 ns decay constant) performs compared to a classic BGO crystal coupled to a PMT (300 ns light decay).

Figure 44 Timing spectrum using a ^{11}C source

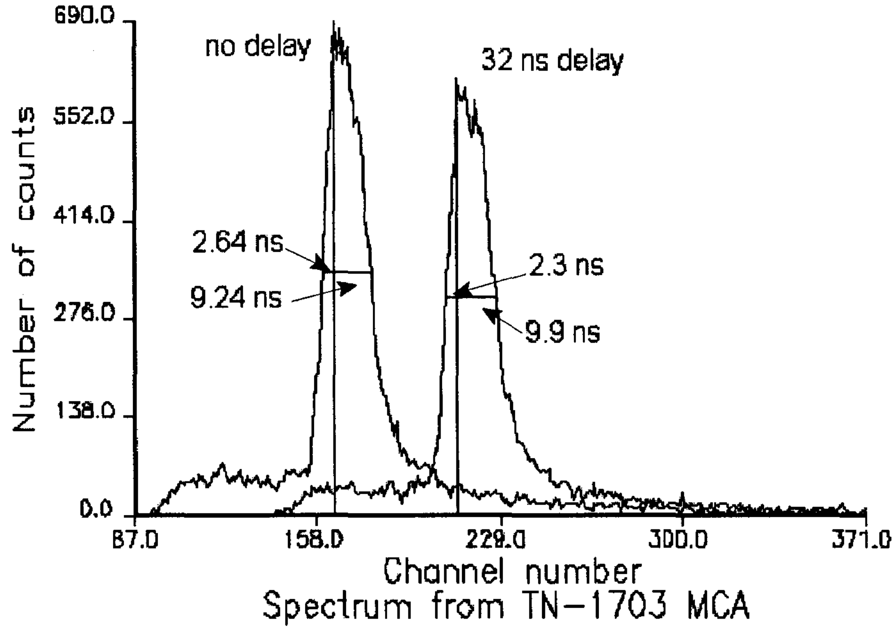

5. Measurement of beta energy spectrum

The positron energy spectrum from ^{11}C acquired with the plastic scintillator detection system is shown in Figure 45. The spectrum decreases almost linearly. Deviations from a linear decrease are expected here due to gamma rays contamination (assumed to be negligible).

Figure 45 Beta spectrum

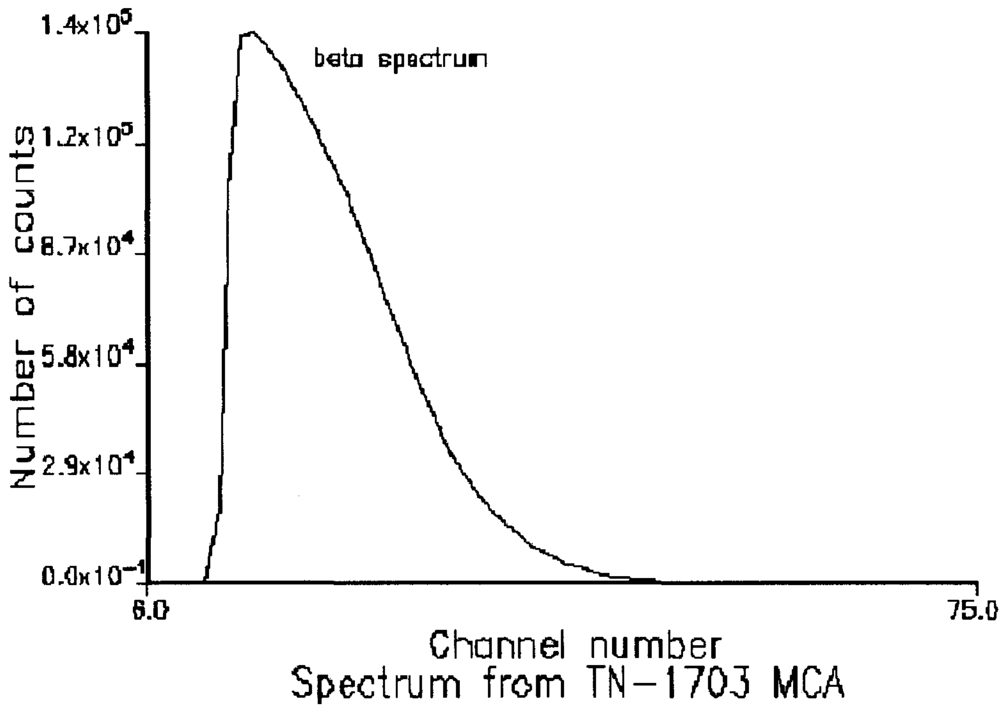

6. Discussion

A new method of attenuation correction in PET has been investigated, using beta-gamma coincidence for transmission scans. In the standard method of transmission scanning using orbiting rod sources the event rate is limited by the count rate of the detector nearest the source. This is not the case with beta-gamma coincidence where the source strength can be increased. With beta-gamma coincidence, the event rate is determined by the sum of the single detectors rates on the far side of the source. This transmission scan method is estimated to be more than a factor of ten faster than orbiting rod sources since it shares the same advantage as the ^{137}Cs single method scan of being able to turn off the nearest detectors [25]. In our technique almost all the near detector photons will have a known origin reducing the need for more precise energy discrimination and longer pulse shaping time. The effects of random events will also decrease thanks to the known locations of the annihilations and this method also allows post-injection scans without adding extra random events. Moreover, in contrast to the ^{137}Cs method, our technique allows multiple sources which enable the entire scan field to be covered..

Comparison with Jones' technique

The technique implemented by Jones *et al.* [30, 31] using a collimated coincidence ^{68}Ge point source with dedicated LSO crystal close by to detect gamma rays gives very encouraging results. The beta-gamma technique shares all the advantages of Jones' technique (higher count rate, lower noise, faster scanning time) as well as having the advantages of being cheaper, faster and more efficient as discussed previously.

New requirements for transmission scans

Whole body oncology scans are performed to stage primary disease, evaluate nodal involvement and identify metastatic spread to other organs. The availability of accurately aligned, whole body functional PET images has a significant impact on the diagnosis and staging of malignant disease and on identifying and localizing metastases. At present PET transmission scans are acquired in 2D with inter-plane septa whereas emission scans are acquired in 3D. Whole body studies require multiple bed positions and for every position a transmission and an emission scan must be performed as explained earlier. In beta-gamma coincidence there is no need for septa and transmission scans are performed in 3D thus decreasing scan time. Moreover the scintillation emission of a typical plastic scintillator has a decay time of 2 ns as opposed to LSO or BGO crystals which have decay times of 42 and

300 ns respectively. This makes plastic scintillators better suited for fast timing and decreased PET detector dead time. Such improved performance rates allow the use of hotter sources, reduce scan time and lower image noise. The encoding time might also be decreased thanks to the non-utilization of the nearest detectors. Finally positron detection has the possibility of decreasing scanner costs due by eliminating the septa and their moving mechanisms. Modern clinical PET requires fast scanning and noise-free transmission scans rather than accuracy of the attenuation coefficients.

Use of other isotopes

Although ^{11}C was used exclusively in the preliminary studies presented here, the use of other isotopes such as ^{18}F and ^{68}Ge has been implemented. ^{68}Ge has the advantage of providing a "permanent" transmission source as opposed to the ^{11}C gel which must be prepared before each run. Plastic scintillator cylinders were manufactured in the McGill University Physics workshop and sent to Sanders Medical Products, Inc. to be filled with ^{68}Ge and sealed. Four sealed source cylinders were received back in mid-September 2001. We also plan to test a source created by imbedding ^{22}Na into the plastic scintillator itself using TISOL (Triumf Isotope Separator On Line) accelerator. These sources are to be manufactured in December 2001.

CONCLUSION

Whole body oncology scans are performed to stage primary disease, evaluate nodal involvement, and identify metastatic spread to other organs. The availability of accurately aligned, whole body functional positron emission tomography (PET) images has a significant impact on the diagnosis and staging of malignant disease and on identifying and localizing metastases. PET is being increasingly used with F-18-fluorodeoxyglucose (FDG) to evaluate recurrent tumors and to stage cancer by assessing the existence of remote tumors as in the case of metastases. The quality of attenuation correction in PET can still be improved. The new method introduced in this thesis, beta-gamma attenuation correction, is very promising as a future improvement for PET. This technique has been tested and successfully implemented on an animal PET scanner. The tests showed that this technique has a good efficiency and very promising timing results.

The work carried out in this thesis included using plastic scintillation fibers for positron detection, electronic design of fast amplifiers, mechanical design and construction of a transmission box and plastic scintillator cylinders and the implementation of a preliminary beta-gamma attenuation correction system on an animal PET scanner. This work represents a necessary first step in the development of this novel technique for performing transmission scans. We now plan on extending the experimental setup from two PMTs to four in order to more effectively cover the crystal area and to solve any undersampling problems which could arise from using a two PMT setup. This extended work requires the construction of two extra pre-amplifiers as well as a significant amount of timing calibration. Finally, the ANIPET reconstruction program has been recently modified to directly use the beta-gamma detection system for attenuation measurements. The new code which performs this is given in Appendix II.

Appendix I [43]

Derivation of noise propagation in PET

It can be shown that the variance in the reconstructed image [44,45]:

$$\sigma^2 \leq \frac{\pi^2 \Delta t}{N_\theta} \sigma_{\max}^2 \int FRF(f)^2 df \quad \text{(A1)}$$

Where Δt is the linear sampling distance, N_θ is the number of angular samples and FRF(f) is the filter function. In the transmission scan, $\sigma_{\max}^2 = 1/I$, where I is the average number of photons detected after transmission through the object. The variance of the attenuation coefficient in the reconstructed image is then:

$$\begin{aligned}
\sigma^2(\mu) &\leq \frac{\pi^2 \Delta t}{N_\theta I} \int FRF(f)^2 df \\
&= \frac{\pi^2 \Delta t N_x}{N_\theta N_x I} \int FRF(f)^2 df \qquad D = N_x \Delta t \quad N_{tot} = N_\theta N_x I \\
&= \frac{\pi^2 D}{N_{tot}} \int FRF(f)^2 df \qquad \text{(A2)}
\end{aligned}$$

Where N_x is the number of linear samples, N_{tot} is the total number of photons passing through the object and D the object diameter. The fractional standard deviation is:

$$\sigma^2(\mu)/\mu^2 \leq \frac{\pi^2 D}{N_{tot}\mu^2} \int FRF(f)^2 df \qquad \text{(A2a)}$$

In the emission scan the detected number of photons, n, is corrected for attenuation by the blank-transmission ratio, I_0/I (i.e. $m = n\, I_0/I$). The corrected number of photons (m) is equal to A (which is the activity concentration times detection efficiency) times the object diameter (D).

$$\sigma^2(m) = \frac{m^2}{I} = \frac{A^2D^2}{I}$$ The variance in the corrected value m is then (assuming no noise in either the blank or emission scan):

$$\sigma^2(A) \leq \frac{\pi^2 \Delta t A^2 D^2 N_x}{N_\theta N_x I} \int FRF(f)^2 df$$ The variance in A is then:

$$= \frac{\pi^2 A^2 D^3}{N_{tot}} \int FRF(f)^2 df$$

(A3)

$$\sigma^2(A) / A^2 \leq \frac{\pi^2 D^3}{N_{tot}} \int FRF(f)^2 df$$ The fractional variance in A:

(A3a)

$$\frac{\sigma_e / A}{\sigma_{tr} / \mu} = D\mu$$ The ratio of the fractional standard deviations is then the square root of the ratio of (A2a) and (A3a) which gives:

(A4)

This is the relationship between the fractional standard deviation in the reconstructed transmission and the corresponding emission scan. In the case for a 22 cm diameter cylinder with an attenuation coefficient of 0.09 cm^{-1} the fractional standard deviation in the attenuation corrected emission scan would be 1.98 times the noise of the transmission scan image.

Appendix II

program written by Dylan D. Togane, revision Sept 6 2001

This program will operate on the parallel projection files generated by Andrew Reader's reconstruction software. One of these is from a blank scan, the other is from the actual transmission scan. It must read in two of these files, by requesting the user to enter their names, and their durations in minutes.

Having read the files into two separate arrays, it will then divide the data in the blank scan by the data in the transmission scan after scaling for the duration and (possibly the isotope decay). The values may be scaled by 1000 to get some initials results. If either number is zero, to output value will be useless, and will be replaced by "1". The values in either array could be replaced by a 3×3 average of the nearest neighbours as an option.

After doing these calculations, a new file should be created which has the same format as the original "pp" file, but a different name. If his file is now reconstructed, the output will be an attenuation map. If data is first converted to natural logarithms, it will provide an attenuation correction file which can later be used to do the attenuation correction.

Program:

```
# include <stdio.h>
# include <string.h>
# include <math.h>
# include <ctype.h>
/*-----------------------------------------------------------------------------------------------*/
typedef struct tag_scan_data
{       char fname [512];
        float duration, rate, *pdata;
}        scan_data;
void read_scan(char *name, scan_data *data);
```

```
/*---------------------------------------------------------------------------------------------------*/
# define YP_DIM 64
# define ZP_DIM 64
# define PHI_DIM 64
# define TH_DIM 5
const int data_len = YP_DIM * ZP_DIM * PHI_DIM * TH_DIM;
const int data_scale = 1000;
/*---------------------------------------------------------------------------------------------------*/
int main (int argc, char *argv [ ] )
{       int ndx;
        char ans [8];
scan_data blank_scan = {0}, trans_scan = {0}, output ={0};
printf ("\n****** ANIPET Attenuation program ******\n\n");
printf ("If uncertain of the isotope decay rates eneter \"1\" for both. \n");
printf ('Otherwise ensure that they are entered in the same units. \n\n");

*/ Read and perform initial processing of blank and transmission scan */
read_scan ("blank", &blank_scan);
read_scan("transmission", &trans_scan);

/* Divide and scale the blank and transmission scans, putting the resulkts in the
transmission scan buffer */
for (ndx = 0; ndx < data_len; ndx ++)
        if (trans_scan.pdata[ndx] != 0 && blank_scan.pdata[ndx] !=0(
        trans_scan.pdata[ndx] / = blank_scan.pdata[ndx];
        else trans_scan.pdata[ndx] = 1.0;
/* Find out whether or not to tke natural logarithms of the output */
printf ("Transform the attenuation map to correction factors by taking \n");
printf ("the natural logarithm? (y or n) \n");
```

```
scanf ("%S", ans);
if (tolower(ans [0] == 'y ') {
        for (ndx=0; ndx <data_len; ndx++)
        trans_scan.pdata[ndx]= log (trans_scan.pdata [ndx] );
}

/* Find out whether to scale the data after division */
printf ("Scale the divided data by %d? (Y or n) \n", data_scale);
scanf("%s", ans);
if (tolower (ans[0] == 'y')
        for (ndx = 0; ndx <data_len; ndx++) trans_scan.pdata[ndx] *=data_scale:

*/ Save the output */
{       char fname [512];
        FILE *f= NULL;
        char *pdot = strrchr (trans_scan.fname, '.'):
        *pdot = '\0';
        sprintf (fname, "%s_atten.p", trans_scan.fname);
        printf ("Saving output to %s \n", fname);
        if (!(f = fopen(fname, "wb"))) {
                char msg [512];
                sprintf (msg, "Error opening file %s", fname);
                perror (msg);
                exit (-1);
        }
        fwrite (trans_scan.pdata, sizeof (float), data_len, f);
        fclose (f);
}
```

```
/*------------------------------------------------------------------------------------------------------------*/
void read_scan (char *name, scan_data *data)
{       FILE *f = NULL;
        char ans [8];
        int ndx;
        printf ("please enter the name of the %s scan: \n", name);
        scanf ("%s", data -> fname);
        data-> pdata = calloc (sizeof (float), data_len);
        if (! (f= fopen (data-> fname, "rb"))) {
                char msg [512];
                sprintf (msg, "Error opening file %s", data-> fname);
                perror (msg);
                exit (-1);
        }
        fread (data->pdata, sizeof (float), data_len, f);
        fclose (f);
        printf("Please eneter the duration (in seconds ) of the %s scan: \ n", name);
        scanf ("%f", &data-> duration);
        printf ("Please eneter the isotope decay rate of the %s scan: \ n", name);
        scanf ("%f", &data-> rate);
        for (ndx = 0; ndx < data_len; ndx++)
                data -> pdata [ndx] / = (data -> duration * data- > rate);
        printf ("Do a 3×3 neasrest-neighbour average of the %s scan? (y or n) \n",name);
        scanf"%s", ans);
        if (tolower (ans [0]) == 'y') {
                int sndx; /* sinogram index */
                float *tmp = calloc (size off (float), YP_DIM *ZP_DIM);
                float *smooth_sino [ZP_DIM];
                for (ndx = 0; ndx < ZP_DIM; ndx ++) smooth_sino [ndx] = &tmp[ndx *
```

```
        YP_DIM];
        for (sndx = 0; sndx < (PHI_DIM * TH_DIM); sndx++) {
            int yndx, zndx;
            float *sino [ZP_DIM];

            /* Get pointers to an individual sinogram */
            for (ndx = 0; ndx <ZP_DIM; ndx ++)
            sino [ndx] = &data -> pdata [(sndx * YP_DIM * ZP_DIM)+ (ndx *
            YP_DIM)];

            / * Do the nearest-neighbour average */
            for (yndx = 1; yndx < (YP_DIM-1); yndx ++) {
            for (zndx = 1 ; zndx < (ZP_DIM-1) zndx++) [
                smooth_sino [zndx] [yndx] += sino [zndx-1] [yndx-1] +
                sino [zndx-1] [yndx] + sino [zndx-1] [yndx+1] + sino [zndx]
                [yndx-1] + sino [zndx] [yndx+1] + sino [zndx+1] [yndx -1]
                + sino [zndx+1] [yndx] + sino sino [zndx+1] [yndx+1];
                smooth_sino [zndx] [yndx] /=9;
            }
            }
            memcpy (&data -> pdata [sndx * YP_DIM *ZP_DIM], tmp,
            sizeof (float) * YP_DIM *ZP_DIM);
            Memset (tmp, 0, sizeof (float) * YP_DIM * ZP_DIM);
    }
    free (tmp);
}
}
```

Here is a sample session where the attenuate program was compiled, linked and run on sample data:

$ cc ATTENUATE .C

$ link ATTENUATE .OBJ

$ r ATTENUATE .EXE

*********ANIPET Attenuation program **********

If uncertain of the isotope decay rates enter "1" for both. Otherwise ensure that they are entered in the same units. Please enter the name of the blank scan :

ani_list:blank.pp

Please enter the duration (in seconds) of the blank scan :

1

Please enter the isotope decay rate of the blank scan:

1

Do a 3×3 nearest-neighbour average of the blank scan? (y or n)

n

Please enter the name of the transmission scan:

ani_list:sino.pp

Please enter the duration (in seconds) of the transmission scan:

1

Please enter the isotope decay rate of the transmission scan:

1

Do a 3×3 nearest-neighbour average of the transmission scan? (y or n)

n

Scale the divided data by 1000? (y or n)

n

Transform the attenuation map to correction factors by taking the natural logarithm? (y or n)

n

Saving output to ani_list:sino_atten.pp

REFERENCES

1. Gullberg G T, Budinger T F. The use of filtering methods to compensate for constant attenuation in single-photon emission computed tomography. *IEEE Trans. Biomed. Eng.* **28:** 142-157 (1981)

2. Figured adapted from :Bergman A. The evaluation of a Positron Emission Mammography System Using Images Co-registered with X-ray Mammograms. *Master's thesis, McGill University, Medical Physics Unit* (1997)

3. Molison R T, Laruelle M, Innis R B. Positron and Single Emission Tomography. In Pschopharmacology: the Fourth Generation of Progress, Ed. FE Bloom and DJ Kupfer, Paven Press Ltd., New York (1995)

4. Cho Z H, Chan J K, Erickson L *et al.* Positron ranges obtained from biomedically important positron emitting radionuclides. *J. Nucl. Med.* **16:** 1174-2276 (1975)

5. Johns E H, Cunnigham J R. The Physics of Radiology fourth ed. Springfield: C. Thomas (1993)

6. Hoffman E J *et al.* Examination of the role of detection systems in quantitation and image quality in PET. *IEEE Trans. Nucl. Sci.* **33:** 420-424 (1986)

7. Ishibashi H. Cerium-doped GSO Scintillator and its applications to Position Sensitive detectors. *IEEE Trans. Nucl. Sci.* **36:**170-172 (1989)

8. Melcher C, Scweitzer J. Cerium-doped luletium oxyorthosilicate: A fast, efficient new scintillator. *IEEE Trans. Nucl. Sci.* **39:** 502-505 (1992)

9. Burle Technologies Inc., Lancaster, PA, *Photomultiplier Handbook.* (1980)

10. Thompson C J, Sciascia P, Murthy K et al. ANIPET a Versatile PET Scanner for Imaging Small Animals. *Paper #M6-33 Proceeding of the 1998 IEEE Medical Imaging Conference, Toronto* (1998)

11. Timing and coincidence counting systems. *Canberra Nuclear Instruments Catalog* edition nine.

12. Benedetti S D, Cowan C, *et al.* On the angular distribution of two-photons annihilation radiation, *Physic Review,* vol. 77. (1950)

13. Ahluwalia B, Positron Emission Imaging, in Nuclear Medical Physics, Vol III, er 2 pp 49-59.

14. Huang S-C, Hoffman E J, Phelps M E *et al.* Quantitation in positron emission computed tomography: 2. Effects of inaccurate attenuation correction. *J. Comput. Assist. Tomogr.* **3:**804-814 (1979)

15. Huang S-C, Carson R E, Phelps M E *et al.* A boundary method for attenuation correction in positron computed tomography. *J. Nucl. Med.* **22:**627-637 (1981)

16. Derenzo S E, Budinger T F, et al:Imaging properties of a positron tomograph with 280 crystals. *IEEE Trans. Nucl. Sci.* **NS-28:** 81-89 (1981)

17. Carroll L R, Kertz P, Orcutt G, The orbiting rod source: Improving performance in PET transmission correction scans. In: "*Emission Computed Tomography; Currents Trends*". New York, Society of Nuclear Medicine, (1983)

18. Kubler W H, Ostertag H, Hoverath H, Doll J, Lorenz W J, Scatter suppression by using a rotating pin source in PET transmission measurements. *IEEE Trans. Nucl. Sci.* **NS-35:** 749-752 (1988)

19. Thompson C J, Ranger N T, Evans A C: Simultaneous transmission and emission scans in positron emission tomography *IEEE Trans. Nucl. Sci.* **36:**1011-1016 (1989)

20. Thompson CJ, Dagher A, Lunney DN, et al. A technique to reject scattered radiation in PET transmission scans. In: International Workshop on Physics and Engineering of Computerized Multidimensional Imaging and Processing Nalcioglu O, Cho ZH, Budinger TF Eds. Proc. SPIE-671:224-253 (1986)

21. Daube-Whitherston M, Carson R E, Green M V. Post-injection transmission attenuation measurements for PET. *IEEE Trans. Nucl. Sci.* **NS-35:**757-761 (1988)

22. Carson R E, Daube-Whitherston M, Green M V. A method for post-injection PET transmission measurements with a rotating source. *J. Nucl. Med.* **29:**1558-1567 (1988)

23. Bailey D L, Hutton B F, Walker P. Improved SPECT using simultaneous emission ans transmission tomography. *J. Nucl. Med.* **28:**844-851 (1987)

24. deKemp R A, Nahamias C. Attenuation correction in PET using single photon transmission measurement. *Med. Phys.* **21:**771-778 (1994)

25. Karp J S, Muehllehner G, Qu H, Yan X H: Singles transmission in volume-imaging PET with a ^{137}Cs source. *Phys. Med. Biol.* **40:**929-944 (1995)

26. Yu S K, Nahamias C: Single-photon transmission measurements in positron emission tomography using ^{137}Cs. *Phys. Med. Biol.* **40:**1255-1266 (1995)

28. Benard F, Smith RJ, Hustinx R, et al. Clinical evaluation of processing techniques for attenuation correction with ^{137}Cs in whole-body PET imaging. *J. Nucl. Med.* **40:**1257-1263 (1999)

29. Smith R J, Karp J S, Benard F, *et al.* A comparaison of segmentation and emission subtraction for singles transmission in PET. *IEEE Tran. Nucl. Sci.* **45:**1212-1218 (1998)

30. Jones W F, Moyers J C, Casey M E, *et al.* Fast -channel LSO detectors and fiber-optic encoding for excellent dual photon transmission measurements in PET. *IEEE Trans. Nucl. Sci* **46:** 979-984 (1999)

31. Watson C C, Eriksson L, Casey M E, *et al.* Design and performance of collimated coincidence point sources for simultaneous transmission measurements in 3D PET. *IEEE Trans. Nucl. Sci* **48:** 673-679

32. Beyer T, Townsend D W, Brun T, *et al.* A combined PET/CT scanner for clinical oncology. *J. Nucl. Med.* **41:** 1369-1379 (2000)

33. Thompson C J, Dagher A, Lunney DN, *et al.* A technique to reject scattered radiation in PET transmission correction scans. In: Nalcioglu O, Cho Z H, Budinger T F, eds. *International workshop on physic and engineering of computerized multidimensional imaging and processing.* Proc. SPIE, **617:** 244-253 (1986)

34. Bengel F M, Ziegler S I, Avril N, *et al.* Whole-body positron emission tomography in clinical oncology: comparaison between attenuation-corrected and uncorrected images. *Eur. J. Nucl. Med.* **24:**1091-1098 (1997)

35. Xu M, Cutler P D, and Luk W K: Adaptive, segmented attenuation correction for whole body PET imaging. *IEEE Trans. Nucl. Sci.* **43:** 331-336 (1996)

36. Riddell C, Brigger P, Carson R E, *et al.* The watersheld algorithm: A method to segment noisy PET transmission scans. *Trans. Nucl. Sci.* **46:** 713-717 (1999)

continuer ici

37. Sorensen JA, Phelps ME. Physics in nuclear medicine. *WB Sanders, Philadelphia* (1987)
38. Thompson CJ, Lecomte R, Cardorette J. Feasibility of using beta-gamma coincidence for 3D attenuation correction. *IEEE Trans. Nucl. Sci.*,**47:** 1176-1181 (2000)
39. Murthy K, Jolly D, Aznar M, et al. Quantification in positron emission mammography (PEM) with planar detectors: Contrast resolution measurements using a custom breast phantom and novel spherical hot-spots. IEEE Trans. Nucl. Sci.,**46:** 2192-2196 (1999)
40. Pain F, Laniece P, Mastrippolito R, *et al.* SIC, an intercerebral radiosensitive probe for in vivo neuropharmacology investigations in small laboratory animals: theoretical considerations and physical characteristics. *IEEE Trans. Nucl. Sci.*,**47:** 25-32 (2000)
41. Jelly J V, Cerenkov Radiation and its Applications, *London: Pergamon* (1958)
42. Jackson J D, Classical Electrodynamics 2nd edn, *New York: Wiley* (1975)
43. Dahlbom M and Hoffman E J, Problems in signal to noise ratio for attenuation correction in high resolution PET. *IEEE Trans. Nucl. Sci.* **NS-34:** 288-293 (1987)
44. Phephs M E, Huang S-C, Hoffman E J, *et al.* An analysis of signal amplification using small detectors in positron emission tomography. *J. Comp. Tomogr.* **6:** 551-565 (1982)
45. Chesler D A, Riederer S J, Pelc N J. Noise due to photon statistics in computed x-ray tomography. *J. Comput. Assit. Tomogr.* **1:** 64-74 (1977)